Polyoxometalates Surrounded by Organic Cations or Immobilized on Functionalized Merrifield Resin as Catalysts for Oxidation of β-Myrcene and β-Caryophyllene

Ali Al Hadi Haidar, Pascal Guillo, Dominique Agustin

applied sciences

MDPI

Article

Polyoxometalates Surrounded by Organic Cations or Immobilized on Functionalized Merrifield Resin as Catalysts for Oxidation of β-Myrcene and β-Caryophyllene

Ali Al Hadi Haidar [1], Pascal Guillo [1,2] and Dominique Agustin [1,2,*]

[1] LCC-CNRS, Université de Toulouse, CNRS, F-31077 Toulouse, France; alialhadi.haidar@lcc-toulouse.fr (A.A.H.H.); pascal.guillo@iut-tlse3.fr (P.G.)
[2] Department of Chemistry, Institut Universitaire de Technologie Toulouse Auch Castres, University of Toulouse, 5 allée du Martinet, F-81100 Castres, France
* Correspondence: dominique.agustin@iut-tlse3.fr; Tel.: +33-5-63-62-11-72

Abstract

Polyoxometalates (POMs) surrounded by organic cations and related systems composed of POMs immobilized on functionalized Merrifield resin (MR) were synthesized, characterized and tested as catalysts for the oxidation of two natural terpenes, β-myrcene and β-caryophyllene, using H_2O_2 and TBHP as green oxidants. The ionic immobilization enabled easy catalyst recovery and reuse. The results showed high conversion and selectivity, with some catalysts maintaining their efficiency for at least three runs without leaching. The catalytic performances of both homogeneous and heterogeneous systems, along with the necessary characterizations, are discussed.

Keywords: polyoxometalates; Merrifield resin; heterogeneous catalysis; organic solvent-free process; biomass valorization

Academic Editor: Raed Abu-Reziq

Received: 13 June 2025
Revised: 12 July 2025
Accepted: 15 July 2025
Published: 17 July 2025

Citation: Haidar, A.A.H.; Guillo, P.; Agustin, D. Polyoxometalates Surrounded by Organic Cations or Immobilized on Functionalized Merrifield Resin as Catalysts for Oxidation of β-Myrcene and β-Caryophyllene. *Appl. Sci.* **2025**, *15*, 7981. https://doi.org/10.3390/app15147981

1. Introduction

The depletion of fossil resources and urgent environmental challenges have accelerated the shift toward renewable biomass as a sustainable feedstock for producing high-value chemicals, materials and fuels [1–4]. Indeed, in line with green chemistry principles, biomass valorization aims to reduce waste, minimize energy consumption and mitigate environmental impacts [5,6]. Among its key transformations, the oxidation of biomass-derived molecules offers routes to fine chemicals for pharmaceuticals, polymers and agrochemicals [7]. In this context, terpenes—as one part of the biomass—are a relevant renewable source for the production of high-value derivatives [8]. This study focuses on two representative terpenes, β-myrcene and β-caryophyllene (Figure 1), chosen for their availability and applications.

β-myrcene is an open-chain monoterpene derived from natural sources [9] or via β-pinene pyrolysis [10]. Its oxidation product, myrcene oxide, is a key intermediate for industrial applications and as an intermediate in the synthesis of fine chemicals, particularly in flavor and fragrance industries [11], as well as in polymer chemistry, enabling the synthesis of bio-based polymers through its reactive epoxide group [10,12–19].

On the other hand, β-caryophyllene, obtained from several sources in essential oils [20], is known for its unique bicyclic structure and biological activity [21,22]. Its oxidation yields β-caryophyllene oxide, a compound of high commercial interest due to its use in fragrances,

cosmetics and pharmaceuticals [22–25], as well as its anti-inflammatory, antimicrobial and anticancer properties [26–28].

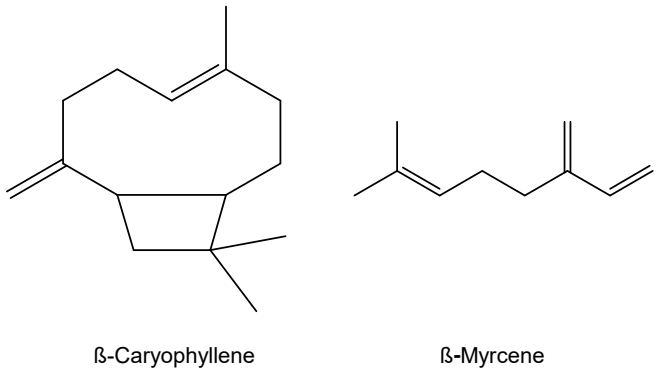

Figure 1. Structures of the evaluated substrates.

Prior oxidation methods for these two terpenes often relied on harsh and non-sustainable conditions. These included toxic oxidants such as chromium(VI) reagents [29], *m*-chloroperbenzoic acid (mCPBA) [18,19,30,31] and even oxone [25,32–34]; most of these processes used hazardous chlorinated solvents such as dichloromethane and chloroform. Additionally, many of these protocols employ expensive and unrecyclable metal-based homogeneous catalysts based on Cu coordination polymers and MOFs [35–37], $MeReO_3$ [38,39], peroxometalates [40–42], biosourced metals [43] and one Lindqvist polyanion [44]. Although quite efficient, most of the cited processes are misaligned with the principles of green chemistry due to the experimental conditions, i.e., non-recyclable catalysts or toxic solvents or reagents.

In our group, we develop organic-solvent-free strategies towards biomass valorization, demonstrating the potential of oxo-molybdenum and oxo-vanadium coordination complexes and polyoxometalates (POMs) as oxidation catalysts for greener transformations [10,12–18]. Notably, Keggin-type POMs, including $[PMo_{12}O_{40}]^{3-}$ and $[PMo_{11}VO_{40}]^{4-}$, offer tunable acidity and redox properties, making them particularly well-suited for oxidation reactions [19–23]. To improve recyclability, these catalysts have been heterogenized via ionic immobilization on solid supports like modified Merrifield resin [45,46] or silica [47,48], achieving recyclable catalytic systems for epoxidation reactions. Merrifield resin (**MR**), a chloromethylated polystyrene-based polymer, stands out as an ideal support due to its commercial availability, low cost, robustness and ease of functionalization, supporting POMs via ionic interactions and preventing leaching while enabling efficient recovery and reuse [49].

Our group has previously demonstrated the successful immobilization of POMs on this support [35], achieving recyclable catalytic systems for the epoxidation of cyclohexene into adipic acid [50].

We present herein the catalytic activity of Keggin-type POMs as organic salts and when immobilized onto functionalized Merrifield resin for the oxidation of both natural substrates, enabling solvent-free oxidation under mild conditions while prioritizing catalyst recyclability.

2. Materials and Methods

2.1. Materials

All materials were used without further purification. Organic solvents (pyridine, acetonitrile, diethyl ether, toluene, ethylacetate, dimethylformamide); β-caryophyllene (Sigma aldrich, St. Louis, MO, USA, >80%); β-caryophyllene oxide (Sigma aldrich, 95%);

β-myrcene (Janssen Chimica, Geel, Belgium, 80%); the corresponding oxides synthesized in the described procedure; and the oxidants H_2O_{2aq} (35%, ACROS), $TBHP_{aq}$ (70% TBHP in water, ACROS), $TBHP_{dec}$ (5-6 M TBHP in decane, Aldrich), naphthalene (99%, Aldrich), 1-butyl pyridinium bromide (Fluka 99%), Butyl methyl imidazolium chloride (synthesized), 1-methyl imidazole (Acros 99%), molybdatophosphoric acid hydrate (Merck), sodium-molybdate dihydrate (99%, Thermo scientific, Waltham, MA, USA), sodium metavanadate (Alfa Aesar, Haverhill, MA, USA), disodium phosphate (Acros 99%), sulfuric acid (95%, Sigma Aldrich) and Merrifield resin (Aldrich, 1.4–1.6 mmol Cl/g) are used as received.

2.2. Methods

Solution NMR: ^{1}H NMR, $^{13}C\{^1H\}$ NMR and $^{31}P\{^1H\}$ NMR spectra were recorded on Bruker (Fällanden, Switzerland) NMR III HD 400 MHz spectrometers, using 400 MHz for ^{1}H NMR, 101 MHz for $^{13}C\{^1H\}$ NMR and 162 MHz for $^{31}P\{^1H\}$ NMR.

Solid NMR: Solid-state NMR: NMR experiments were recorded on Bruker Avance (Fällanden, Switzerland) 400 III HD spectrometers operating at magnetic fields of 9.4 T. Samples were packed into 4 mm zirconia rotors. The rotors were spun at 8 kHz at 293 K. ^{1}H MAS was performed with the DEPTH pulse sequence and a relaxation delay of 3 s. For ^{29}Si MAS single pulse experiments, small flip angles of 30° were used with recycle delays of 60 s. ^{13}C CP and ^{29}Si CP MAS spectra were recorded with a recycle delay of 2 s and contact times of 3 ms and 4 ms, respectively. Chemical shifts use TMS as reference. All spectra were fitted using the DMfit software (version 20190125).

Elemental analysis: Elemental analyses (EAs) were performed by the LCC microanalysis service on PerkinElmer 2400 série II (Waltham, MA, USA).

Infrared: Infrared spectra were recorded using the ATR technique with a Perkin Elmer FTIR/FIR 400 spectrometer with a 4 cm^{-1} resolution and 8 scans.

Gas chromatography: The catalytic reactions were followed by gas chromatography (GC) on an Agilent (Santa Clara, CA, USA) 7820A chromatograph equipped with an FID detector, a DB-WAX capillary column (30 m × 0.32 mm × 0.5 μm) and an autosampler. Conversion and oxide formation were calculated from the calibration curves (R^2 = 0.999) and naphthalene as an internal standard.

2.3. Synthesis of Objects

2.3.1. Heteropolyacid (HPA) Synthesis [51]

$H_4PMo_{11}V_1O_{40}$ was synthesized according to the published procedure. Na_2HPO_4 (3.55 g, 25 mmol) and $NaVO_3$ (sodium metavanadate) (3.1 g, 25 mmol) were mixed in water (20 mL). The mixture was cooled and 3 mL of concentrated sulfuric acid was added. After the addition of 66.5 g (274 mmol) of $Na_2MoO_4{\cdot}2H_2O$, 30 mL of concentrated sulfuric acid was slowly added under vigorous stirring. $H_4PMo_{11}V_1O_{40}$ was extracted with diethyl ether, then recrystallized in water and air dried. A total of 13 g was collected as orange crystals. Yield: 23% IR (ATR, ν(cm^{-1})): 1055–1100 (P-O), 1000–900 (M-O), 850–700 (M-O-M). $^{31}P\{^1H]$ NMR (162 MHz, DMSO-d_6, ppm) δ: −1 (minor), −4.11 (major).

2.3.2. General Synthesis of Organic Salts of POMs

Organic salts of POMs were synthesized by mixing the corresponding heteropolyacid with x equivalent of Butyl methyl imidazolium chloride, or 1-butyl pyridinium bromide in water. The salt formed was filtered then dried after washing with water.

$(BmIm)_3PMo_{12}O_{40}$: $H_3PMo_{12}O_{40}{\cdot}21H_2O$ (1 g, 0.45 mmol) was mixed with 1-butyl-3-methyl imidazolium chloride (0.29 g, 1.3 mmol) in 10 mL water at room temperature for 4 h. The light green salt formed was filtered and dried under vacuum. Yield: 94%. $(C_8H_{15}N_2)_3PMo_{12}O_{40}$ Anal. Calc: C, 12.87; H, 2.03; N,3.75. Found: C, 13.03; H, 1.56; N, 3.87. IR (ATR, ν(cm^{-1})): 3150–2850 (CH), 1563 (C=C), 1460 (C-N), 1060 (P-O), 953 (Mo=O), 780

(Mo-O-Mo). ^{1}H NMR (400 MHz, DMSO-d_6) δ = 9.1 (s, 1H, NCHN), 7.78 (s, 1H, NCH), 7.72 (s, 1H, NCH), 4.21 (t, *J* = 7.1 Hz, 2H, NCH_2), 3.89 (s, 3H, NCH_3), 1.81(m, 2H, CH_2), 1.25 (dq, *J* = 14.7, 7.3 Hz, 2H, CH_2), 0.91 (t, *J* = 7.4 Hz, 3H, but-CH_3). ^{13}C{^{1}H} NMR (101 MHz, DMSO-d_6) δ = 136.94, 124.12, 122.75, 48.99, 36.19, 31.86, 19.25, 13.76. ^{31}P{^{1}H} NMR (162 MHz, DMSO-d_6) δ = −1.36 (minor), −4.11 (major).

(BmIm)$_4$PMo$_{11}$VO$_{40}$: $H_4PMo_{11}VO_{40}\cdot 28H_2O$ (1 g, 0.43 mmol) was mixed with 1-butyl-3-methyl imidazolium chloride (0.38 g, 1.7 mmol) in 10 mL water at room temperature for 4 h. The yellow salt formed was filtered and dried under vacuum. Yield: 94%. $(C_8H_{15}N_2)_4PMo_{11}VO_{40}$ Anal. Calc: C, 16.47; H, 2.59; N,4.8. Found: C, 16.95; H, 1.97, N, 4.78. IR (ATR, ν(cm^{-1})): 3150–2850 (CH), 1568 (C=C), 1466 (C-N), 1063 (P-O), 953 (Mo=O), 740–880 (M-O-M). ^{1}H NMR (400 MHz, DMSO-d_6) δ = 9.1 (s, 1H, NCHN), 7.76 (s,1H, NCH), 7.7 (s, 1H, NCH), 4.21 (t, *J* = 7.1 Hz, 2H, NCH_2), 3.85 (s, 3H, NCH_3), 1.77 (m, 2H, CH_2), 1.27 (dq, *J* = 14.7, 7.3 Hz, 2H, CH_2), 0.91 (t, *J* = 7.4 Hz, 3H, but-CH_3). ^{13}C{^{1}H} NMR (101 MHz, DMSO-d_6) δ = 136.94, 124.12, 122.75, 48.99, 36.19, 31.86, 19.25, 13.76. ^{31}P{^{1}H} NMR (162 MHz, DMSO-d_6) δ = −1.35 (minor), −4.60 (major).

(BuPyr)$_3$PMo$_{12}$O$_{40}$: $H_3PMo_{12}O_{40}\cdot 21H_2O$ (1 g, 0.45 mmol) was mixed with 1-butyl pyridinium bromide (0.28 g, 1.3 mmol) in 10 mL water at room temperature for 4 h. The light green salt formed was filtered and dried under vacuum. Yield: 95%. $(C_9H_{14}N)_3PMo_{12}O_{40}$ Anal. Calc: C, 16.5; H, 1.8; N, 1.88. Found: C, 18.36; H, 1.85; N, 2.49. IR (ATR, ν(cm^{-1})): 3150–2850 (CH), 1632 (C=C), 1485 (C-N), 1061 (P-O), 951 (Mo=O), 740–880 (Mo-O-Mo). ^{1}H NMR (400 MHz, DMSO-d_6) δ = 9.10 (d, *J* = 5.4 Hz, 1H, 2H, Py-CHN), 8.6 (t, *J* = 7.9 Hz, 1H, Py-CH), 8.18 (t, *J* = 7.1 Hz, 2H, Pyr-CH), 4.62 (t, *J* = 7.5 Hz, 2H, NCH_2), 1.92 (m, 2H, CH_2), 1.31 (m, 2H, CH_2), 0.93 (t, *J* = 7.3 Hz, 3H but-CH_3). ^{13}C{^{1}H} NMR (101 MHz, DMSO-d_6) δ = 145.71, 144.94, 128.35, 60.89, 32.91, 19.02, 13.56. ^{31}P{^{1}H} NMR (162 MHz, DMSO-d_6) δ = −1.33 (minor), −4.13 (major).

(BuPyr)$_4$PMo$_{11}$VO$_{40}$: $H_4PMo_{11}VO_{40}\cdot 28H_2O$ (1 g, 0.43 mmol) was mixed with 1-butyl pyridinium bromide (0.37 g, 1.7 mmol) in 10 mL water at room temperature for 4 h. The yellow salt formed was filtered and dried under vacuum. Yield: 90%. $(C_9H_{14}N)_4PMo_{11}VO_{40}$ Anal. Calc: C, 15; H, 1.9; N, 1.91. Found: C, 15.71; H, 1.93; N, 2.11. IR (ATR, ν(cm^{-1})): 3150–2850 (CH), 1629 (C=C), 1485 (C-N), 1054 (P-O), 947 (Mo=O), 740–880 (Mo-O-Mo). ^{1}H NMR (400 MHz, DMSO-d_6) δ = 9.00 (d, *J* = 5.4 Hz, 2H, Py-CHN), 8.52 (t, *J* = 7.8 Hz, 1H, Py-CH), 8.08 (t, *J* = 7.1 Hz, 2H, Py-CH), 4.52 (t, *J* = 7.4 Hz, 2H, NCH_2), 1.82 (m, 2H, CH_2), 1.20 (m, 2H CH_2), 0.83 (t, *J* = 7.3 Hz, but-CH_3). ^{13}C{^{1}H} NMR (101 MHz, DMSO-d_6) δ = 145.7, 144.92, 128.33, 60.89, 32.91, 19.02, 13.56. ^{31}P{^{1}H} NMR (162 MHz, DMSO-d^6) δ = −4.12 (minor), −4.6 (major).

2.3.3. **MR@Org** and **MROrg@POMs** Synthesis [52]

MR@Org synthesis: **MR** (1.4–1.6 mmol Cl/g, 4 g) was stirred with 1-methylimidazole (0.048 mol, 4 g) or pyridine (0.05 mol, 4 g) in DMF (20 mL) at 80 °C for 24 h, followed by being washed with dichloromethane to remove unreacted organic compounds. **MR@Imd** (4 g) and **MR@Pyr** (4 g) were obtained as a pale beige powder.

MR@Pyr: IR (ATR, ν(cm^{-1})): 3050–3100 (C-H), 2910 (C-H), 1630 (C-N), 1484 (C=C), 700–800 (C-H aromatic). E.A: C: 40.27%, H: 8.8%, N: 2.26%.

MR@Imd: IR (ATR, ν(cm^{-1})): 3050–3100 (C-H), 2910 (C-H), 1616 (N-H), 1332 (C-N) 1155 (C-H). E.A: C: 39.86%, H: 8.71%, N: 4.25%.

MROrg@POMs synthesis: The functionalized **MR@Org** was grafted with POMs by mixing them in an aqueous solution.

For **MRImd@PMo$_{12}$O$_{40}$** and **MRPyr@PMo$_{12}$O$_{40}$**, 2 g of **MR@Imd** or **MR@Pyr** was mixed with 2.2 g (1 mmol) of **H$_3$PMo$_{12}$O$_{40}$** in water and then filtered, washed with water and dichloromethane and finally dried under vacuum.

For **MRImd@PMo$_{11}$VO$_{40}$** and **MRPyr@PMo$_{11}$VO$_{40}$**, (2 g) of **MR@Imd** or **MR@Pyr** was mixed with 1.8 g of **H$_4$PMo$_{11}$VO$_{40}$** (0.8 mmol) then filtered, washed with water and dichloromethane and finally dried under vacuum.

IR (ATR, ν(cm^{-1})) for all grafted POMs: 1055–1100 (P-O), 1000–900 (M-O), 850–700 (M-O-M).

MRImd@PMo$_{12}$O$_{40}$: Olive-green color. EA: C: 33.13%, H: 2.63%, N: 3.49%, TGA (0–600 °C): 81%. ^{1}H MAS: 7.29, 3.37, 1.1. ^{13}C MAS: 146.14, 136.27, 128.74, 53.19, 45.56, 40.11, 36.77. ^{31}P MAS: −0.23, −1.95, −4.0 (major).

MRImd@PMo$_{11}$VO$_{40}$: Sepia color. EA: C: 38.55%, H: 3.3%, N: 4.1%, TGA (0–600 °C): 80%. ^{1}H MAS: 7.25, 3.89, 1.13. ^{13}C MAS: 145.81, 128.50, 53.05, 43.89, 40.11, 36.53. ^{31}P MAS: −4.28.

MRPyr@PMo$_{12}$O$_{40}$: Olive-green color. EA: C: 31.74%, H: 1.75%, N: 1.78%, TGA (0–600 °C): 77.8%. ^{1}H MAS: 8.12, 3.77. ^{13}C MAS: 144, 128.96, 64.82, 44.76, 40.27, 9.40. ^{31}P MAS: −0.22, −2.40, −4.1 (major).

MRPyr@PMo$_{11}$VO$_{40}$: Sepia color. EA: C: 37.02%, H: 2.39%, N: 2.04%, TGA (0–600 °C): 76.6%. ^{1}H MAS: 7.99, 3.55. ^{13}C MAS: 144.53, 128.98, 64.9, 43.93, 39.96, 9.44. ^{31}P MAS: −4.46.

2.3.4. Synthesis of β-Myrcene Oxide (7-8-Epoxy β-Myrcene) [53]

β-myrcene oxide was synthesized according to the described procedure. ^{1}H NMR (400 MHz, $CDCl_3$) δ = 6.38 (dd, *J* = 10.6, 17.6 Hz, 1H, CH), 5.25 (d, *J* = 17.6 Hz, 1H, CH), 5.09 (d, *J* = 10.6 Hz, 1H, CH), 5.05 (s, 1H, CH), 5.04 (s, 1H, CH), 2.76 (t, *J* = 6.3 Hz, 1H, CH_2), 2.41 (m, 1H, CH_2), 2.36 (m, 1H, CH_2), 1.75 (m, 2H, CH2), δ 1.31 (s, 3H, CH_3), δ 1.26 (s, 3H, CH_3).

2.4. Catalytic Oxidation Procedure

With **Org@POMs**

In a typical experiment, β-myrcene (1.36 g, 0.01 mol) or β-caryophyllene (2.04 g, 0.01 mol), naphthalene as an internal standard (0.04 g) and **Org@POMs** (2.5×10^{-5} mol) were mixed in a round bottom flask. According to the nature of the oxidant, once the reaction temperature regulated as defined (80 °C with $TBHP_{aq}$ and $TBHP_{dec}$ and 70 °C with H_2O_{2aq}), 2 equivalents of oxidant ($TBHP_{aq}$, $TBHP_{dec}$ or H_2O_2 in water, with/without addition of toluene or ethylacetate) were added to start the reaction. The reaction mixture was left under stirring for 5 h in both cases. Samples of the organic phase of the reaction mixture were withdrawn periodically and injected into the GC. The quantification was performed using naphthalene as an internal standard and calibration curves.

With **MROrg@POMs**

In a typical experiment, β-myrcene (1.36 g, 0.01 mol) or β-caryophyllene (2.04 g, 0.01 mol), naphthalene as internal standard (0.04 g) and 0.1 g of **MROrg@POMs** (corresponding to 5×10^{-5} mol of POM) were mixed in a round bottom flask. According to the nature of the oxidant, once the reaction temperature regulated as defined (80 °C with $TBHP_{aq}$ and $TBHP_{dec}$ and 70 °C with H_2O_{2aq}), 2 equivalents of oxidant ($TBHP_{aq}$, $TBHP_{dec}$ or H_2O_2 in water, with/without addition of toluene or ethylacetate) were added to start the reaction. The reaction mixture was left under stirring for 5 h in both cases. Samples of the organic phase of the reaction mixture were withdrawn periodically and injected into the GC. The quantification was performed using naphthalene as an internal standard and calibration curves with the GC error for both Conv and Yield (±2%).

Conversion and yields are calculated according to the following equations:

Conv (%) = $[(n_{(sub)t0} - n_{(sub)5h})/n_{(sub)t0}] \times 100$ and Oxide yield (%) = $[n_{(oxide)5h}/n_{(sub)t0}] \times 100$ where (sub) β-myrcene or β-caryophyllene and (oxide) is the corresponding oxide product.

3. Results and Discussion

3.1. Synthetic Pathways of the Catalysts

3.1.1. Molecular POMs with Organic Cations

In order to compare the catalytic activity of homogeneous catalysts and their supported version, POMs (based on $H_3PMo_{12}O_{40}$ and $H_4PMo_{11}VO_{40}$ as heteropolyacid (HPA) precursors) surrounded with organic moieties were synthetized, mimicking the surface of the targeted support. 1-butyl pyridinium bromide (BuPyrBr) or butyl-methyl imidazolium bromide (BmImBr) reacted with HPAs in water in an OrgBr/HPA ratio of 3:1 with $H_3PMo_{12}O_{40}$ and 4:1 in the case of $H_4PMo_{11}VO_{40}$ (Figure 2). Salts precipitate and are isolated as colored powders in ca. 95% yield. POMs with the organic cations **$(Org)_3PMo_{12}O_{40}$** and **$(Org)_4PMo_{11}VO_{40}$** (Org = BuPyr or BmIm) are the molecular versions of the grafted ones.

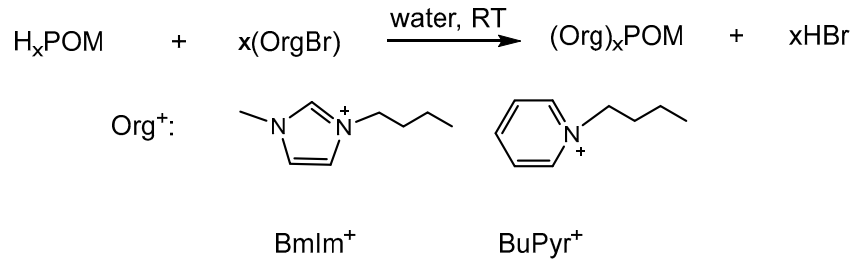

Figure 2. $(Org)_3PMo_{12}O_{40}$ and **$(Org)_4PMo_{11}VO_{40}$** synthesis scheme.

3.1.2. Immobilized POMs on Functionalized MRs

The synthesis of the immobilized catalytic systems was achieved in two steps, as described in Scheme 1 by the modification of a previously reported procedure [52]. Initially, in order to introduce a cationic moiety, Merrifield resin (**MR**) was functionalized via the quaternization of the chloromethylated function using either 1-methylimidazole (Imd) or pyridine (Pyr) as quaternizing agents. **MR@Org** was obtained (Org: methylimidazole, Imd or pyridine, Pyr) as pale beige powders.

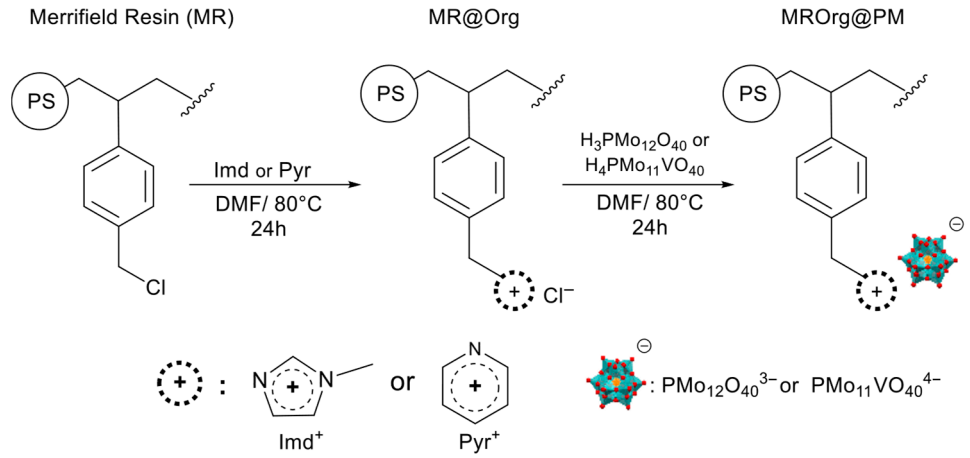

Scheme 1. Synthetic pathway of immobilized catalysts.

In the second step (Scheme 1), **$MROrg@PMo_{12}O_{40}$** was obtained by mixing **MR@Org** (Org = Pyr or Imd) with an aqueous solution of heteropolyacids (HPAs) ($H_3PMo_{12}O_{40}$ or $H_4PMo_{11}VO_{40}$), leading to **$MRImd@PMo_{12}O_{40}$** and **$MRPyr@PMo_{12}O_{40}$** as an olive-green powder and **$MRImd@PMo_{11}VO_{40}$** and **$MRPyr@PMo_{11}VO_{40}$** as a sepia powder. All these catalytic objects were characterized before their use in catalysis.

3.2. Characterization of the Catalysts

3.2.1. Molecular POMs with Organic Cations

- *IR characterization*

The IR spectra of the organic salts of POMs (Figure 3), **$(Org)_3PMo_{12}O_{40}$** and **$(Org)_4PMo_{11}VO_{40}$** (Org = BuPyr or BmIm), present characteristic peaks confirming the presence of polyoxometalate (POM) structures and organic functional groups. The Mo=O stretching vibrations appear around 950–970 cm^{-1}, while the Mo-O-Mo bridging vibrations are observed in the range of 750–880 cm^{-1}. The presence of BuPyr and BmIm cations is indicated by C-H stretching bands in the 2800–3100 cm^{-1} region, along with C=N or aromatic ring vibrations near 1600 cm^{-1} [51].

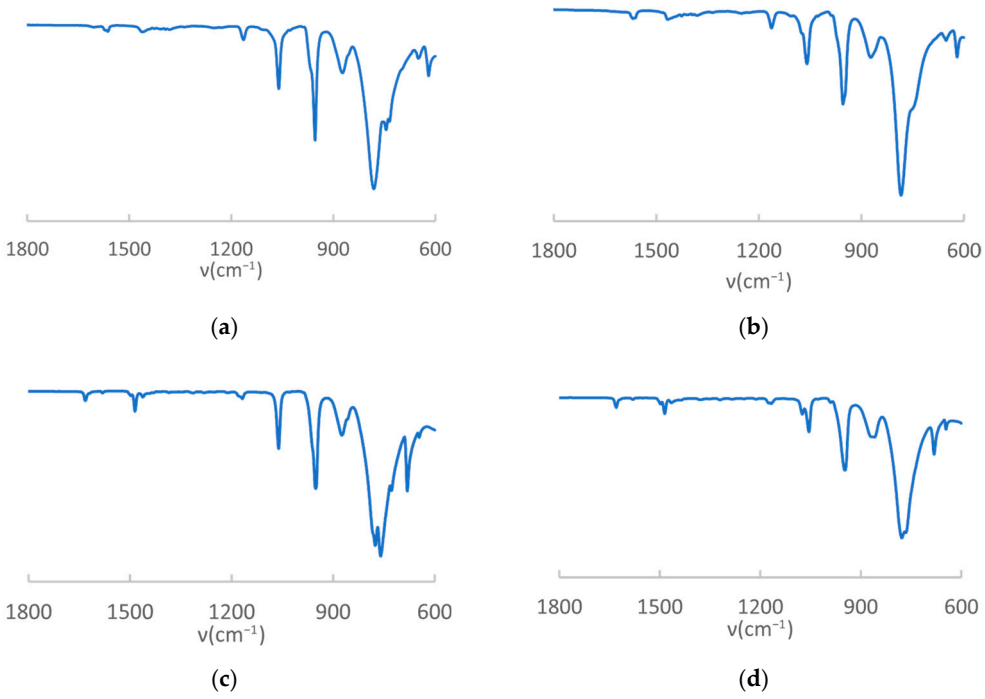

Figure 3. IR spectra of organic salts of POMs. (**a**): $(BmIm)_3PMo_{12}O_{40}$, (**b**): $(BmIm)_4PMo_{11}VO_{40}$, (**c**): $(BuPyr)_3PMo_{12}O_{40}$ and (**d**): $(BuPyr)_4PMo_{11}VO_{40}$.

For better comparison, the range of the IR spectrum in Figure 3 is restricted to the region of interest. Full spectra are in the SI.

3.2.2. Immobilized POMs on Functionalized MRs

- *IR Characterization of **MR@Org***

The IR spectra of **MR@Imd** and **MR@Pyr** (Figure 4) exhibit several key peaks that confirm the successful grafting of the imidazolium and pyridinium groups. Broad absorption bands observed in the 3100–3500 cm^{-1} range correspond to N-H and C-H stretching vibrations, characteristic of imidazolium and pyridinium rings. The presence of peaks around 1600–1700 cm^{-1} likely indicates C=N and C=C stretching. Additionally, multiple peaks in the fingerprint region (500–1500 cm^{-1}) suggest vibrations associated with the grafted functional groups [54].

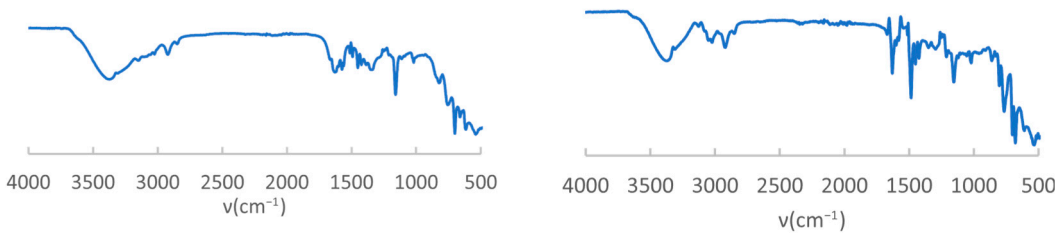

(**a**) (**b**)

Figure 4. IR spectra of (**a**) **MR@Imd** and (**b**) **MR@Pyr**.

- *Quantification of the functional groups on **MR@Org***

The quantification of functional groups (Imd or Pyr) (Table 1) on the modified **MR** was essential before the immobilization of the POMs on the **MR@Org** surfaces. This quantification was possible by the determination of the N content of the **MR@Org** objects by elemental analysis. As described in Table 1, the content of the organic moieties (in mmol per g of **MR@Org**) is 1.5 and 1.6 for Imd and Pyr, respectively. Considering the Cl content of the **MR** (indicated to be 1.4–1.6 mmol/g), the values of Imd and Pyr indicate full substitution.

Table 1. Imd and Pyr content on MROrg and POM loading on MR@POM.

	Imd or Pyr Content (mmol/g MR) [1]		**POM Loading (mmol/g of MR@POM)** [2]
MR@Imd	1.5	**MRIm@PMo$_{12}$O$_{40}$**	0.444
		MRIm@PMo$_{11}$VO$_{40}$	0.402
MR@Pyr	1.6	**MRPyr@PMo$_{12}$O$_{40}$**	0.426
		MRPyr@PMo$_{11}$VO$_{40}$	0.43

[1] from E.A and [2] from TGA.

- *Quantification of POM loading on **MROrg@POM***

Based on these results, an accurate quantity of POMs was added for their immobilization on **MR@Org**. POM loading could be determined from TGA experiments (Table 1), with the remaining residue after 400 °C being attributed to the POM content.

Compared to our previous work [52], the quaternization procedure significantly improved the accessibility of POMs to the ionically functionalized moieties. This enhancement resulted in POM loadings ranging from 0.40 to 0.44 mmol per gram of Merrifield resin (**MR**), which was substantially higher than the maximum loading of 66.7 µmol/g reported previously.

- *IR Analysis of **MROrg@POM***

The successful immobilization of POMs on **MR@Org** was clearly demonstrated by IR spectroscopy, as shown in Figure 5. The IR spectra in orange correspond to either $H_3PMo_{12}O_{40}$ or $H_4PMo_{11}VO_{40}$, and those in blue correspond to the difference between **MROrg@POM** and **MR@Org** IR spectra (see the figure affiliation). Indeed, the characteristic vibrations attributed to POMs clearly indicated their presence at the surface of the materials. In particular, a shoulder at 1055–1100 cm^{-1} corresponds to P–O vibrations, a sharp peak at 1000–900 cm^{-1} is attributed to Mo–O stretching and metal–oxygen–metal bridging interactions are observed in the 850–700 cm^{-1} region. The expected V–O absorption may be masked by overlapping Mo–O vibrations [51]. Also, a small peak observed around 1600 cm^{-1} may be attributed to C=N stretching, and may originate from the pyridine and methylimidazole groups grafted onto it, which is further confirmed by elemental analysis (EA).

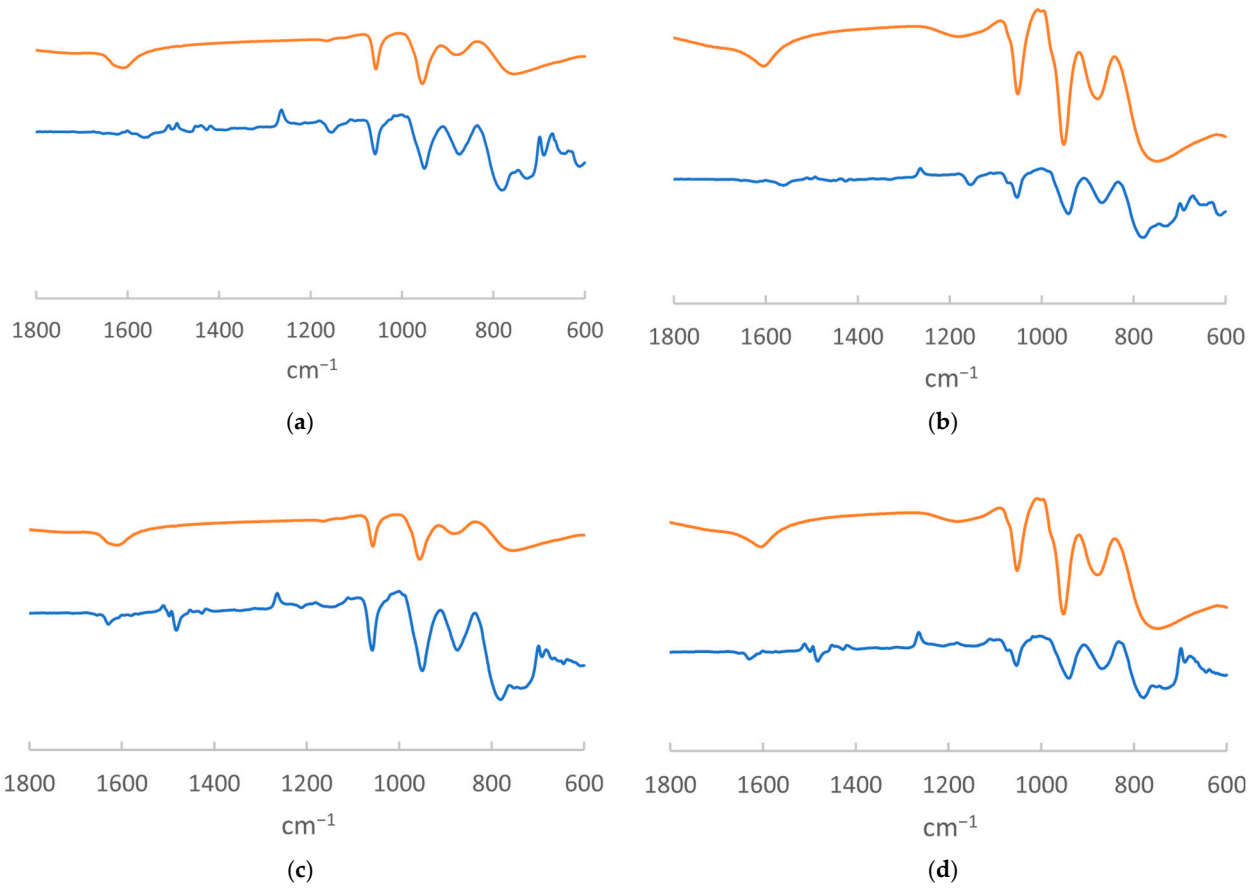

Figure 5. IR spectra: in orange: POMs and in blue: substraction of spectra. (**a**) In orange $H_3PMo_{12}O_{40}$ and in blue **MRImd@PMo$_{12}$O$_{40}$—MR@Imd;** (**b**) in orange $H_4PMo_{11}VO_{40}$ and in blue **MRImd@PMo$_{11}$VO$_{40}$—MR@Imd;** (**c**) in orange $H_3PMo_{12}O_{40}$ and in blue **MRPyr@PMo$_{12}$O$_{40}$—MR@Pyr;** (**d**) in orange $H_4PMo_{11}VO_{40}$ and in blue **MRPyr@PMo$_{11}$VO$_{40}$—MR@Pyr**.

3.3. Swelling Test of Merrifield Resin with β-Myrcene

To assess the accessibility and compatibility of the substrate within the **MR** polymeric system under organic-solvent-free conditions during the catalytic act, preliminary swelling tests were conducted on untreated **MR**. When heated at the reaction temperature in the presence of β-myrcene, the **MR** exhibited a mass increase of around 8% after 5 h, indicating possible substrate incorporation into the polymer pores. This confirms the substrate accessibility without the need for an organic solvent, supporting the use of **MR** as a support for the solvent-free approach [55].

3.4. Catalyzed Oxidation of β-Myrcene

The literature describes that the oxidation of myrcene mainly leads to the formation of myrcene oxide (6,7-epoxide) (Scheme 2) [10,56]. Both 1,2- and 3,10-epoxide may be obtained (not detected in our case) with a lower stability compared to 6,7-epoxide which is the most substituted epoxide. Under these conditions, a Diels–Alder cycloaddition side reaction may also occur, leading to the formation of camphorene as a secondary product, as shown below (Scheme 2) [13]. It has to be noted that myrcene polymerizes at low temperatures, even if air is excluded, making the control of the oxidation process more challenging [57–59].

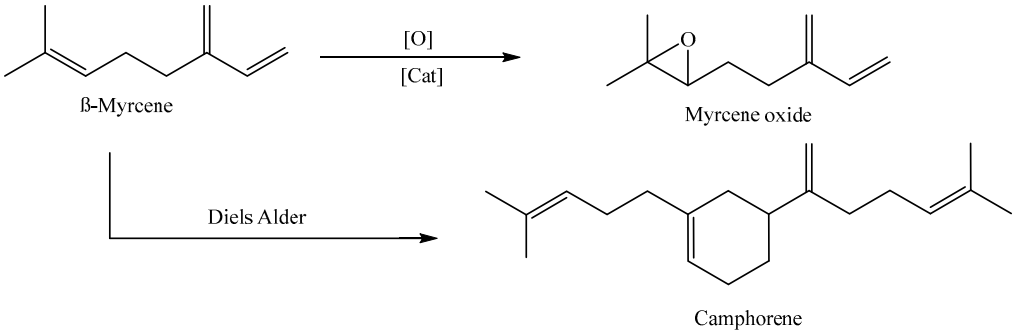

Scheme 2. β-myrcene oxidation scheme with the main products identified in this study.

3.4.1. General Experimental Considerations

The oxidation of β-myrcene was conducted for 5 h with a POM/myrcene/oxidant molar ratio (the POM being an organic salt of the POM described later) of 0.25/100/200, using two different temperatures due to the nature of the oxidant, i.e., at 80 °C with TBHP (in water or decane) and 70 °C with H_2O_2. In some cases, solvent (toluene or ethyl acetate) was added with H_2O_2. With **MROrg@POMs**, 0.1 g was employed, corresponding to a POM/myrcene/oxidant molar ratio of 0.25×10^{-3}/100/200 under similar temperature and time conditions with $TBHP_{aq}$ and H_2O_2. The reaction was followed using GC and using naphthalene as an internal standard. Reactions were repeated three times and were reproducible with a 5% error range. All results have been summarized in Table 2.

Table 2. β-myrcene oxidation catalytic results.

Catalysts	Entry	T (°C)	Oxidant	β-Myrcene Conv (%)	Myrcene Oxide Yield (%)
None	M1	80	None	47 [2]	DA *
$(BmIm)_3PMo_{12}O_{40}$	M2	70	H_2O_{2aq}	75	1
	M3	70	H_2O_{2aq} + Toluene	82	29
	M4	80	$TBHP_{aq}$	40	7
	M5	80	$TBHP_{dec}$	89	39
$(BuPyr)_3PMo_{12}O_{40}$	M6	70	H_2O_{2aq}	79	2
	M7	70	H_2O_{2aq} + Toluene	29	2
	M8	80	$TBHP_{aq}$	60	10
	M9	80	$TBHP_{dec}$	80	15
$(BmIm)_4PMo_{11}VO_{40}$	M10	70	H_2O_{2aq}	87	7
	M11	70	H_2O_{2aq} + Toluene	87	28
	M12	70	H_2O_{2aq} + EtOAc	95	2
	M13	70	H_2O_{2aq} + EtOAc + CH_3CN [1]	94	2
	M14	80	$TBHP_{aq}$	81	53
	M15	80	$TBHP_{dec}$	88	41
$(BmIm)_4PMo_{11}VO_{40}$	M16	80	NNone	37 [2]	
	M17	40	H_2O_{2aq}	20	5
	M18	40	$TBHP_{aq}$	24	4
$(BuPyr)_4PMo_{11}VO_{40}$	M19	70	H_2O_{2aq}	75	1
	M20	70	H_2O_{2aq} + Toluene	26	2
	M21	80	$TBHP_{aq}$	70	41
	M22	80	$TBHP_{dec}$	85	9
Naked **MR**	M23	70	H_2O_{2aq}	47	
	M24	80	$TBHP_{aq}$	42	
	M25	80	$TBHP_{dec}$	39	

Table 2. *Cont.*

Catalysts	Entry	T (°C)	Oxidant	β-Myrcene Conv (%)	Myrcene Oxide Yield (%)
MRImd@PMo$_{12}$O$_{40}$	M26	70	H_2O_{2aq}	94	6
	M27	80	$TBHP_{aq}$	64	6
MRPyr@PMo$_{12}$O$_{40}$	M28	70	H_2O_{2aq}	94	5
	M29	80	$TBHP_{aq}$	95	5
MRImd@PMo$_{11}$VO$_{40}$	M30	70	H_2O_{2aq}	98	9
	M31	80	$TBHP_{aq}$	88	9
	M32	80	$TBHP_{dec}$	75	26
MRPyr@PMo$_{11}$VO$_{40}$	M33	70	H_2O_{2aq}	95	5
	M34	80	$TBHP_{aq}$	85	5

[1] Few drops of CH_3CN were added. [2] β-myrcene was heated without oxidant. DA *: Diels–Alder product detected in GC-MS. Catalytic conditions: For ionic salts of POMs: cat/sub/ox: 0.25/100/200, and at 80 °C with $TBHP_{aq}$ and $TBHP_{dec}$ and at 70 °C with H_2O_{2aq} for 5 h. Toluene and ethyl acetate were added as solvents with H_2O_{2aq} in some cases. For grafted POMs: 0.1 g of **MROrg@POMs** was used in which cat/sub/ox were 0.25 × 10^{-3}/100/200, and at 80 °C with $TBHP_{aq}$ and at 70 °C with H_2O_{2aq} for 5 h.

3.4.2. Effect of H_2O_2 as Oxidant with Organic Salts of POMs

H_2O_2 and a catalyst are needed to form the epoxide. At 80 °C without the oxidant (M16) or in the presence of the **(BmIm)$_4$PMo$_{11}$VO$_{40}$** catalyst only (M1), no myrcene oxide was formed. Temperature is also important. Indeed, with this catalyst, at 40 °C (M17), oxidation was observed with 5% oxide formation and with low conversion. At 70 °C (Entries M2, M6, M10, M19), β-myrcene conversion values ranged from 75% (M2) to 87% (M10), depending on the catalyst composition. Oxide formation was minimal in each case (maximum of 7% for M10) under these conditions, suggesting that H_2O_2 in water at this temperature promoted hydroxylation. Polymerization or Diels–Alder condensation was also possible (camphorene being observed in GC-MS).

The miscibility between the substrates and the expected products as well as the reaction media could also alter the observed reactivity. To assess this hypothesis, different solvents were evaluated. The addition of toluene was tested with the four catalysts (Entries M3, M7, M11, M20). With BmIm salts, conversion was identical to or better than when under organic-solvent-free conditions and oxide yield was higher (close to 28% vs. 1% without toluene). With the BuPyr salts, conversion dropped and the conversion was not significantly enhanced. The difference in reactivity observed by the addition of toluene is unknown but probably has to be linked to the difference in the solubility of catalysts in toluene. Best results were obtained using toluene as a solvent since reactions with EtOAc (M12) or a EtOAc/CH_3CN mixture (M13) led to highest conversion (>94%) but very low selectivity towards the epoxide. According to the precedents in such transformations, acetonitrile could be a suitable solvent with H_2O_2 to enhance the oxide formation, but this was not the case herein [22].

The high quantity of unknown products might be linked to the nature of the substrate itself. Indeed, as stated earlier, myrcene tends to condensate, including camphorene. This is probably what was observed when the reaction was performed without a catalyst and with no oxidant (M1), with 47% conversion, leading to several products including camphorene (detected in GC-MS). Similar behavior was observed in the presence of **(BmIm)$_4$PMo$_{11}$VO$_{40}$** but without an oxidant (M16), with 37% conversion.

3.4.3. Effect of TBHP as Oxidant with Organic Salts of POMs

Using $TBHP_{aq}$, similar or lower conversions were observed in comparison to H_2O_{2aq}, but this was associated with a significant increase in myrcene oxide yields in all cases, being

in the range of 7–10% (M4 and M8) in the case of $(PMo_{12}O_{40})^{3-}$ and 41–53% (M21, M14) for the $(PMo_{11}VO_{40})^{4-}$ salts; the highest yield was for the BmIm salt.

The highest conversion was obtained for all salts when using TBHP in decane, proving the positive role of apolar and aprotic solvents. In terms of yields towards myrcene oxide, the best results are obtained with **$(BmIm)_3PMo_{12}O_{40}$** (39% yield, M4) and **$(BmIm)_4PMo_{11}VO_{40}$** (41% yield, M15) as catalysts.

TBHP seems to be more effective for epoxidation than H_2O_2. This is certainly due to the fact that TBHP is more soluble in apolar organic media. With TBHP in decane ($TBHP_{dec}$), conversion improved further in all cases (Entries M4, M15 and M9) with good oxide yields in the cases of BmIm salts compared to BuPyr ones. For example, 89% conversion with a 39% yield of oxide was obtained with **$(BmIm)_3PMo_{12}O_{40}$** (Entry M5), which was much higher than that with the same POM. However, within the other organic part, a high conversion (80%) but lower yield of oxide (15%) was observed (Entry M9).

On the other hand, with the best-chosen conditions and with $TBHP_{dec}$, only 39% conversion was observed with naked **MR** (Entry M25), with no oxide formed, which could be due to the Diels–Alder reaction (as described before), highlighting the crucial role of the POM in the oxide formation process.

3.4.4. Effect of H_2O_2 as Oxidant with Immobilized POMs

With H_2O_2 as the oxidant, all immobilized catalysts (Entries M26, M28, M30 and M33) demonstrated better myrcene conversion (94–98%) than related organic salts. Although low (5–9%), all yields towards myrcene oxide were higher than those for related organic salts. We can postulate that the interaction with the organic part of the resin stabilizes the oxide and does not lead to the ring opening, but the Diels–Alder reaction seems to still be present, as proved by the experiment using **MR** only (M23).

3.4.5. Effect of TBHP as Oxidant with Immobilized POMs

In contrast, with $TBHP_{aq}$, oxide formation was lower than with the related organic salts (5–9%), despite there being higher conversion in all cases (Entries M27, M32, M29 and M34).

This could be due to the restricted accessibility of TBHP molecules to the active sites or a different activation mechanism influenced by the resin matrix.

One test was performed with TBHP in decane, and, surprisingly, the yield was high, although the conversion was lower (Entry M32). Thus, the compatibility between the substrate and the oxidant seems to be the main factor in the formation of oxide. Otherwise, the competition between oxidation and Diels–Alder was won by the latter, as we proved with both types of TBHP and the 40% conversion observed (Entries M24 and M25).

The performance of Entry M32 is likely due to the better solubility of TBHP in an organic phase and the better solubility of the substrate in $TBHP_{dec}$, leading to a more efficient oxidation process and making it a promising candidate for recyclable catalysis. Due to its high conversion, selectivity and activity with $TBHP_{dec}$, this condition was chosen for the recyclability test (see Section 3.6).

3.4.6. Diels–Alder Investigation

As explained previously, the Diels–Alder reaction was expected to be the most important side reaction for the oxidation of β-myrcene [13,59]. Indeed, as observed during catalytic experiments, even under oxidative conditions, only a minor part of the substrate was converted into its corresponding oxide. The experiments clearly demonstrated that β-myrcene underwent a Diels–Alder dimerization at 80 °C in the absence of any catalyst or oxidant. This was confirmed by GC-MS analysis, which identified the dimerization product and showed no evidence of oxide formation, despite a 47% conversion of β-myrcene

(Entry M1). Interestingly, when **(BmIm)$_4$PMo$_{11}$VO$_{40}$** was used without an oxidant, the conversion dropped from 47% (Entry M19) to 37% after catalyst addition (Entry M20), suggesting that the catalyst interacted with β-myrcene and somehow slowed down the dimerization process.

3.5. β-Caryophyllene Oxidation

3.5.1. General Experimental Considerations

The oxidation of β-caryophyllene was performed for 5 h with a POM/caryophyllene/oxidant molar ratio of 0.25/100/200 at 80 °C using TBHP as an oxidant and at 70 °C with H_2O_2 as an oxidant. In some cases, toluene or ethyl acetate was added as a solvent with H_2O_2. For the immobilized POMs, 0.1 g of a Merrifield-resin-supported catalyst (**MROrg@POMs**) was employed, with a 0.25 × 10^{-3}/100/200 POM/caryophyllene/oxidant molar ratio, under similar temperature conditions according to the nature of the oxidant. The reaction was monitored over time and quantified using GC-FID and using naphthalene as an internal standard. All relevant data have been collected in Table 3.

Table 3. Catalytic results of epoxidation of β-caryophyllene.

Catalysts	Entry	T (°C)	Conditions	β-Caryo [1] Conv (%)	Oxide Yield (%)
(BmIm)$_3$PMo$_{12}$O$_{40}$	C1	70	H_2O_{2aq}	98	26
	C2	80	$TBHP_{aq}$	98	45
(BuPyr)$_3$PMo$_{12}$O$_{40}$	C3	70	H_2O_{2aq}	98	14
	C4	80	$TBHP_{aq}$	98	24
(BmIm)$_4$PMo$_{11}$VO$_{40}$	C5	70	H_2O_{2aq}	99	40
	C6	80	H_2O_{2aq} + EtOAc	99	57
	C7	80	$TBHP_{aq}$	98	64
	C8	70	$TBHP_{dec}$	98	66
(BuPyr)$_4$PMo$_{11}$VO$_{40}$	C9	70	H_2O_{2aq}	99	15
	C10	70	H_2O_{2aq} + EtOAc	92	42
	C11	80	$TBHP_{aq}$	99	31
	C12	80	$TBHP_{dec}$	99	36
Naked **MR**	C13	70	H_2O_{2aq}	5	-
	C14	80	$TBHP_{aq}$	5	-
	C15	80	$TBHP_{dec}$	11	-
MRImd@PMo$_{11}$VO$_{40}$	C16	70	H_2O_{2aq}	94	36
	C17	80	$TBHP_{aq}$	92	62
	C18	80	$TBHP_{dec}$	94	62
MRImd@PMo$_{11}$VO$_{40}$ Catalyst removal after 1 h *	C19	80	$TBHP_{aq}$	62	20
	C20			71	21

[1]: β-caryophyllene. *: The reaction was conducted for 1 h with cat, then for the remaining 4 h after catalyst filtration. Catalysis conditions: For ionic salts of POMs: cat/sub/ox: 0.25/100/200, and at 80 °C with $TBHP_{aq}$ and $TBHP_{dec}$ and at 70 °C with H_2O_{2aq} for 5 h. Toluene and ethyl acetate were added as solvents with H_2O_{2aq} in some cases. For grafted POMs: 0.1 g of **MROrg@POMs** was used, in which cat/sub/ox: 0.25 × 10^{-3}/100/200, and at 80 °C with $TBHP_{aq}$ and $TBHP_{dec}$ and at 70 °C with H_2O_{2aq} for 5 h.

The oxidation of β-caryophyllene leads primarily to the formation of β-caryophyllene oxide, a bicyclic sesquiterpene commonly found in various plants and essential oils [60,61]. This study will focus on this oxide.

3.5.2. Effect of H_2O_2 as Oxidant with Organic Salts of POMs

In comparison to β-myrcene, β-caryophyllene exhibited a higher oxidation efficiency under all tested conditions and was mainly oxidized to its corresponding more stable oxide, as shown in Scheme 3 [27]. With H_2O_{2aq}, conversion values consistently reached 97–99% in all the tested cases (Entries C1, C3, C7 and C9). However, the formation of the oxide was strongly dependent on the catalyst composition. Once again, BuPyr-based catalysts produced lower oxide yields (14–15%) (Entries C7 and C9), with higher yields in the case of BmIm salts (26% (Entry C1) and 40% (Entry C5)), highlighting the possible steric or solubility differences between the organic salts.

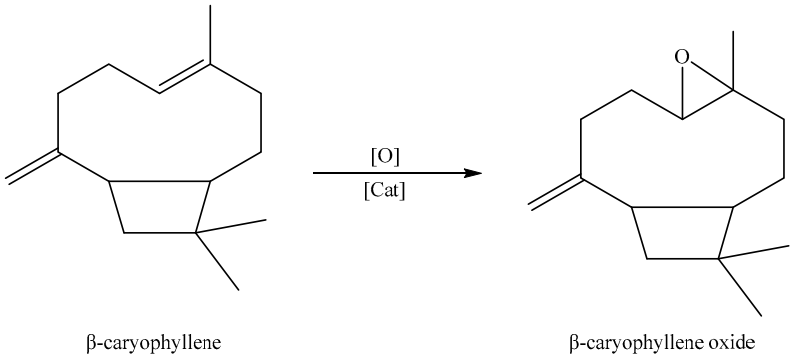

Scheme 3. β-caryophyllene oxidation scheme.

3.5.3. Effect of TBHP as Oxidant with Organic Salts of POMs

When using aqueous TBHP as the oxidant, a similar trend was observed, with consistently high conversions (~97–99%) across all tested conditions (Entries C2, C4, C7 and C11). However, oxide formation was significantly higher, ranging from 30% to 62%. Notably, the catalyst **$(BmIm)_4PMo_{11}VO_{40}$** achieved 64–66% oxide formation (Entry C7), nearly double that observed with aqueous H_2O_2. In contrast, **$(BmIm)_3PMo_{12}O_{40}$** gave lower oxide yields under the same conditions (45% in Entry C2).

Overall, all systems tested with $TBHP_{aq}$ led to very good oxide yields, highlighting the strong influence of both the oxidant and the catalyst structure on the reaction outcome. The use of $TBHP_{dec}$ further increased oxide selectivity (66%) (Entry C8) when compared to $TBHP_{aq}$ (64%), and the same trend was also observed in Entries C11 and C12, which suggests that nonpolar environments favor epoxide formation.

3.5.4. Solvent Influence

In contrast to the oxidation of β-myrcene, the addition of ethyl acetate led to high conversion (99%) and enhanced oxide formation (57%) with **$(BmIm)_4PMo_{11}VO_{40}$** (Entry C6). The rigid structure of β-caryophyllene may lead to more selective oxidation, as the steric constraints limit unwanted side reactions. The effect was even more pronounced with BuPyr catalysts, with oxide formation (42%, Entry C10) higher than in the organic-solvent-free condition (15%, Entry C9). This highlights once again the substrate-dependence selectivity and the effect of the solvent.

The same trend was also observed in the case of $TBHP_{dec}$. The oxide yields increased in both tested cases (Entries C8 and C12), showing slightly higher yields than in the case of $TBHP_{aq}$ (Entries C7 and C11), which may be caused by the higher solubility in the decane and *tert*-butanol produced as a by-product.

In addition, a maximum of 11% of conversion was obtained with naked **MR**, confirming the crucial role of the POMs in the transformation, which was also seen in the case of β-myrcene.

3.5.5. Effect of H_2O_2 as Oxidant with Immobilized POMs

Only **MRImd@PMo$_{11}$V$_1$O$_{40}$**, whose homogeneous analog has demonstrated higher reactivity, was evaluated.

With H_2O_2, the tested grafted catalyst that had the highest efficient selective oxidation showed behavior almost similar to its non-grafted counterparts, with slightly lower conversion in the grafted form (Entries C5 and C16).

3.5.6. Effect of TBHP as Oxidant with Immobilized POMs

With $TBHP_{aq}$, oxide formation was the same in both cases (grafted and non-grafted) and the same formations were obtained in the two cases (62%) (Entries C7 and C17), with slightly lower conversion in the grafted form. In addition, the use of $TBHP_{dec}$ with β-caryophyllene also yielded the best overall oxidation performance, with 98% conversion and 66% oxide formation (Entry C8), with the same tested catalyst in both grafted and non-grafted forms.

3.5.7. Leaching Experiment with **MRImd@PMo$_{11}$VO$_{40}$**

Before evaluating the recyclability of the supported catalysts, leaching experiments have been conducted (Table 3, Entries C19 and C20 and Figure 6) in order to assess the nature of the catalytic process (homogeneous or heterogeneous). Based on the oxidation of β-caryophyllene, two reactions were conducted using **MRImd@PMo$_{11}$VO$_{40}$** as a catalyst and $TBHP_{aq}$ as an oxidant. The first one has been conducted under classical conditions: 5 h at 80 °C ("unfiltered reaction" in gray). For the second reaction, after 1 h, the catalyst was removed by filtration ("filtered reaction" in blue) and the resulting reaction mixture was maintained at 80 °C under stirring for 4 h. For the unfiltered reaction, both the conversion of β-caryophyllene and oxide yields increased between 1 h and 5 h (from 62% to 92% for the conversion and from 20% to 62% for the oxide yields, Entries C17 and C19). Concerning the filtered reaction, a slight increase in the conversion was observed between 1 h and 5 h (from 62% to 71%, Entries C19 and C20) but no oxide was formed after the filtration of the catalyst (Entries C19 and C20).

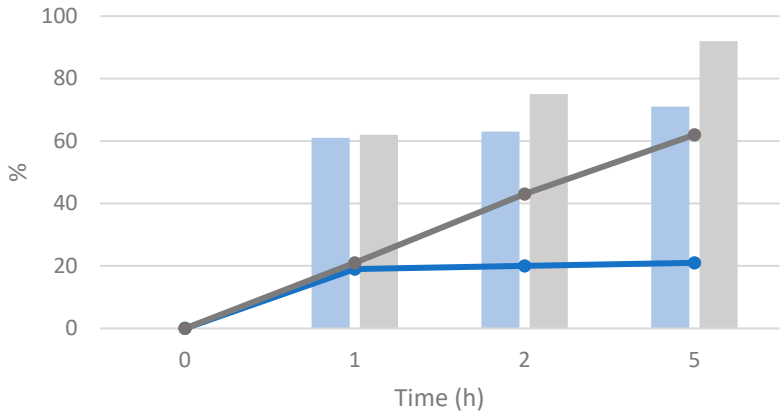

Figure 6. Leaching experiment test for the oxidation of β-caryophyllene with **MRImd@PMo$_{11}$VO$_{40}$** as a catalyst and $TBHP_{aq}$ as an oxidant. Bars correspond to the conversion of β-caryophyllene (gray: unfiltered reaction, blue: filtered reaction after 1 h) reactions. Line graphs correspond to the yields of the oxide form (dark gray: unfiltered reaction, dark blue: filtered reaction after 1 h).

Based on the slight increase in β-caryophyllene conversion, leaching of the POM might be initially envisioned. However, no phosphorous-based species was detected by liquid $^{31}P\{^1H\}$ NMR of the filtrate and the formation of the oxide stopped after filtration. In addition, the oxide could not be obtained without the presence of the catalyst, as proved by

the naked **MR** reaction (Entries C13 and C14). Altogether, the results clearly indicate that no leaching occurred into the reaction mixture.

The difference in conversion observed between 1 h and 5 h may be attributed to the swelling behavior of the polymer support, as previously demonstrated in the swelling test. Additionally, side reactions—such as those identified in control experiments using unmodified Merrifield resin—could also contribute to this variation.

3.6. Recyclability of the Catalysts with Both Substrates and ***MRImd@PMo$_{11}$VO$_{40}$***

Recyclability experiments were realized with **MRImd@PMo$_{11}$VO$_{40}$**, the catalyst displaying the best conversion/yield under the optimized tested conditions (5 h with TBHP$_{aq}$ as oxidant). After the first catalytic experiment, the reaction mixture was filtered and the resulting solid was washed with ethyl acetate, then dried to be reused. By applying the same condition reactions, no decrease in the yields and conversions of both evaluated substrates were observed after three cycles (Figure 7).

Imd@PMo$_{11}$VO$_{40}$ maintained the same performance in three consecutive runs with the same β-myrcene conversion (75%) and with 25% β-myrcene oxide formation.

Promising results were also obtained with **MRImd@PMo$_{11}$VO$_{40}$** for β-caryophyllene oxidation, with constant conversion (92%) and oxide yields (60%) after each of the three runs, and thus without any leaching being obtained, as described in the leaching experiment.

This highlights the stability of the grafted catalyst and its stability under oxidative condition reactions. Also, as confirmed by the leaching test previously described, the absence of catalyst leaching supported its stability. These results highlight the strong durability and reusability of the catalyst, making it a valuable tool for terpene oxidation.

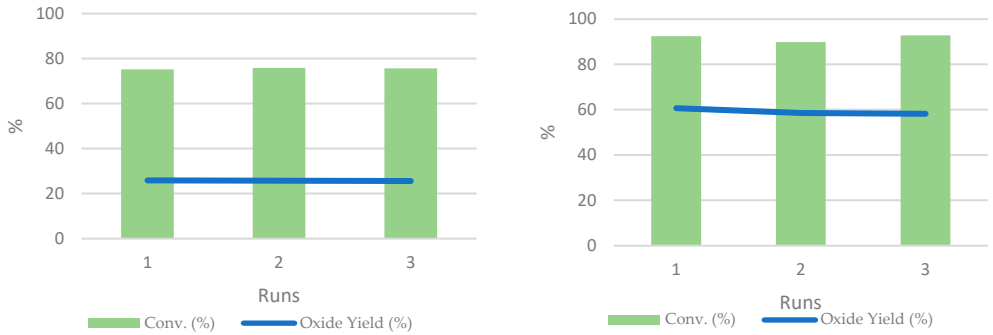

(**a**) (**b**)

Figure 7. Recyclability tests using **MRImd@PMo$_{11}$VO$_{40}$** as catalyst for (**a**) β-myrcene oxidation and (**b**) β-caryophyllene oxidation. Green bars: conversion (%) and blue line: oxide yield (%).

The stability of the catalyst was also evaluated by solid-state NMR by conducting ^{31}P and ^{13}C MAS NMR experiments on the catalysts before and after catalysis. Only minor structural modifications upon reuse were observed (Figure 8), indicating the good stability of the catalyst. Notably, the ^{31}P MAS NMR spectra (a and c) displayed a sharp peak at −4.29 ppm, which remained unchanged after three catalytic cycles (−4.28 ppm). This is also confirmed in the ^{13}C MAS NMR spectra (b and d), with the main peak at around 128.7 ppm still present. Some minor changes may be observed, perhaps due to the adsorption of organic species, which may contribute to minor structural modifications. Thus, the spectra suggested that the overall structure of the catalyst remained preserved. However, while the catalyst retained its main structural features, some surface modifications or partial deactivations may occur upon reuse.

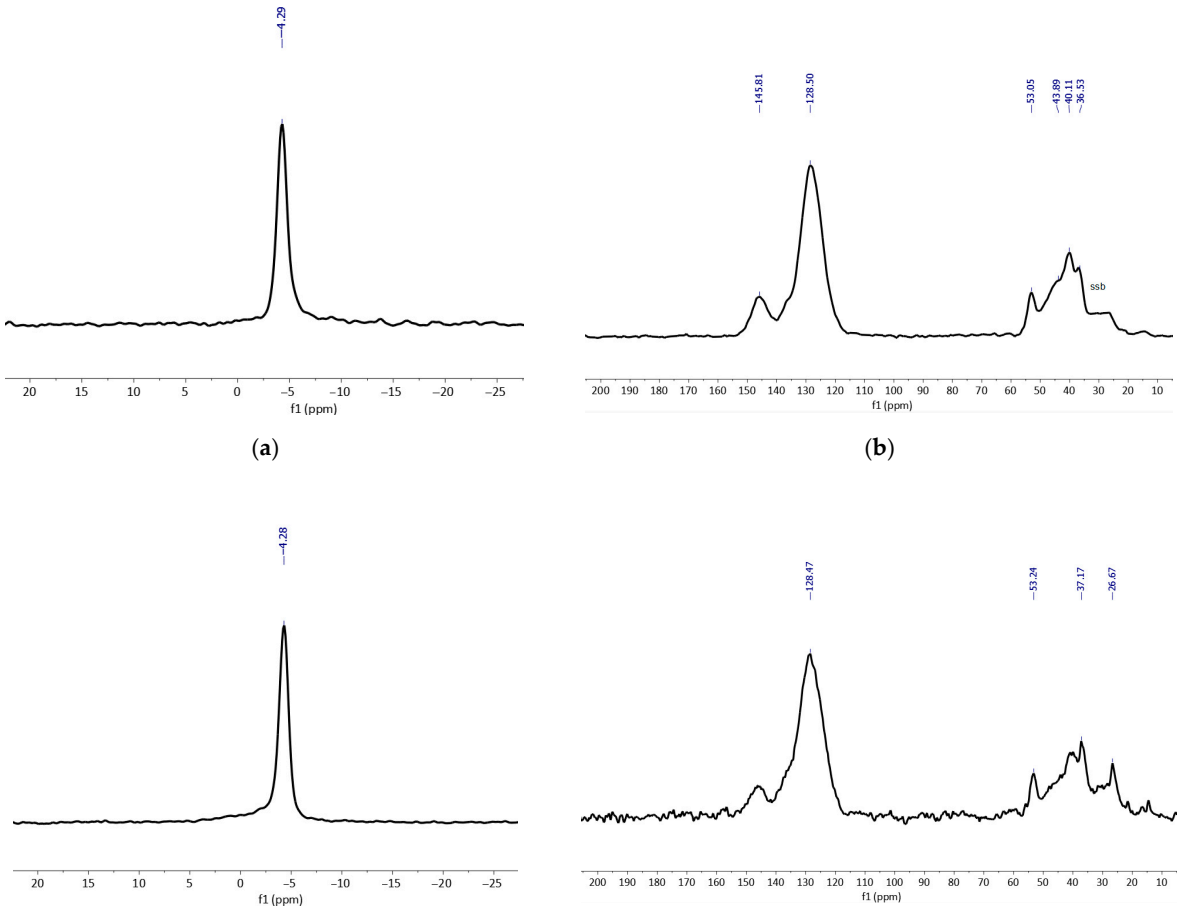

Figure 8. ^{31}P and ^{13}C MAS NMR spectra of **MRImd@PMo$_{11}$VO$_{40}$** before (**a**,**b**) and after the three catalytic runs (**c**,**d**).

3.7. Effect of Tert-Butanol on Oxidation—A Putative Explanation

Tert-butanol (TBA) is commonly used as a co-solvent in oxidation reactions due to its ability to stabilize reactive oxygen species and prevent undesired radical chain reactions. Herein, TBA appeared as a side product in TBHP-based oxidation reactions. The impact of *tert*-butanol can be analyzed based on the observed trends in conversion efficiency and oxide formation in the TBHP$_{aq}$ and TBHP$_{dec}$ systems [62].

Reactions using TBHP exhibited different selectivity compared to H_2O_{2aq}. It is well known that polyoxometalates (POMs) undergo partial decomposition or structural transformation in the presence of peroxides such as H_2O_2. This process often leads to the formation of lower molecular weight oxo or peroxo species, which may exhibit enhanced catalytic activity due to the increased accessibility of the metal centers and the formation of more reactive intermediates. However, the presence of *tert*-butanol in these oxidation reactions can help to stabilize the POM structure under such oxidative conditions. *Tert*-butanol is known to moderate the reactivity of hydrogen peroxide and suppress radical-induced decomposition, thereby supporting the persistence of catalytically active peroxo species while minimizing the structural degradation of the POM framework. Hence, TBHP led to significantly higher oxide formation, particularly with vanadium-substituted catalysts [63]. It is commonly accepted that the reaction mechanism with some oxo-metals and with TBHP accepts peroxide coordination to metal-oxo species (Mo, W, V, Ti) with the formation of tBuOO-M, with such species being less destabilized by the presence of tBuOH. This is in

contrast with H_2O_2 which might evolve to an M-OOH species, transforming into M(O_2) which is considered to be less reactive [53–55] (Scheme 4).

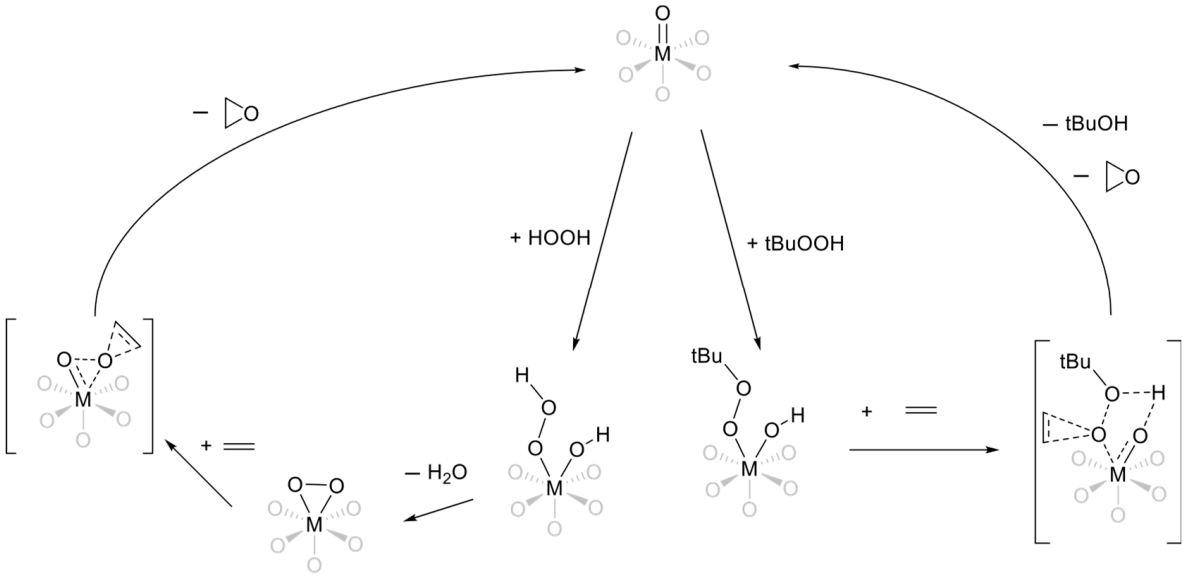

Scheme 4. Putative reactivity according to the nature of the oxidant.

3.8. Green Metric Considerations

The green metrics (AE: Atom Efficiency, RME: Reaction Mass Efficiency, MRP: Mass Recovery Percentage, 1/SF: 1 over the Stoichiometric Factor) were calculated according to a previous published article [64].

The graphs of Figure 9 illustrate the assessment of green chemistry metrics for the oxidation of β-myrcene (a) and β-caryophyllene (b) under different reaction conditions. A wider distribution in the radar plots signifies a greener process, while a more squeezed shape indicates lower performance in terms of the considered green parameters.

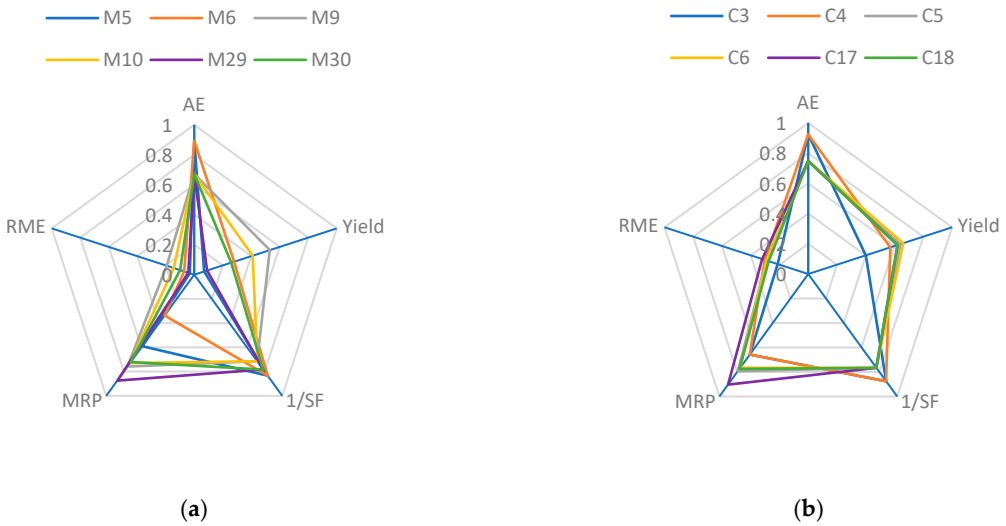

(**a**) (**b**)

Figure 9. Radial distribution with green matrix of **(BmIm)$_4$PMo$_{11}$VO$_{40}$** with β-myrcene (**a**) and β-caryophyllene (**b**) for different entries in different conditions, where blue (H_2O_{2aq}), orange (H_2O_{2aq} + solvent; toluene in (**a**) and ethyl acetate in (**b**)), gray ($TBHP_{aq}$), yellow ($TBHP_{dec}$), purple (grafted form (**MRImd@PMo$_{11}$VO$_{40}$**) with $TBHP_{aq}$) and green (grafted form (**MRImd@PMo$_{11}$VO$_{40}$**) with $TBHP_{dec}$) are presented.

In the case of β-myrcene, the gray curve (M9, $TBHP_{aq}$) stands out with the best atom economy and the highest yield. However, despite its efficiency, the catalyst was not recovered, making the process less sustainable. In contrast, the grafted catalyst with $TBHP_{dec}$ (green) showed improved catalyst recovery but at the cost of a slightly lower yield, demonstrating a trade-off between recyclability and reaction efficiency. The same behavior can be observed between M5 (H_2O_{2aq}) and M6 (H_2O_{2aq} + toluene) where better yields cost lower MRPs and have more waste. The side reactions in β-myrcene oxidation affected the metrics, further constraining the green profile.

On the other hand, for β-caryophyllene oxidation, all processes displayed better green metrics, with blue (H_2O_{2aq}) being the least efficient, yielding the lowest values in both the yield and sustainability parameters. Notably, the grafted catalyst with $TBHP_{aq}$ (C17, purple) exhibited similar yields to the $TBHP_{dec}$ (C18, green) system but with significantly improved mass recovery (MRP), emphasizing its advantage in catalyst recyclability. These results highlight that for greener oxidation, the grafted catalyst, particularly with aqueous $TBHP_{aq}$, offers a balance between efficiency and sustainability, making it a more environmentally friendly alternative, especially in such transformations with limited side reactions. This demonstrates that such products can be obtained with green procedures involving catalyst recovery and reuse.

4. Conclusions

This study demonstrated the efficient oxidation of two natural terpenes, β-myrcene and β-caryophyllene, using Keggin-type polyoxometalates primarily based on molybdenum and vanadium surrounded by organic cations. These POMs were successfully grafted onto Merrifield resin (**MR**) functionalized with organic groups analogous to those in the ionic salts, yielding heterogeneous catalysts with excellent catalytic properties.

Among the studied catalysts, **MRImd@PMo$_{11}$VO$_{40}$**, featuring imidazolium as the organic cation and a vanadium-substituted POM, exhibited superior performance. This superiority was evident for both terpenes, achieving very good conversions with high selectivity toward valuable oxidation products. To the best of our knowledge, this is the first time that V-containing POMs have achieved such transformations with those substrates.

The catalytic oxidation utilized the benign oxidants hydrogen peroxide (H_2O_2) and tert-butyl hydroperoxide (TBHP) under solvent-free and green conditions, aligning with sustainable biomass valorization principles. The ionic immobilization on **MR** allowed easy catalyst recovery and reuse, with the grafted catalysts maintaining their activity and selectivity over at least three consecutive cycles without detectable leaching.

Overall, the results highlight the promising potential of organic-salt-modified and POM-grafted Merrifield resin catalysts for selective terpene oxidation, combining efficient conversion, high selectivity, catalyst recyclability and environmentally friendly process conditions. The comparative analysis of homogeneous versus heterogeneous systems underscores the advantages of the immobilized catalysts in practical applications.

Supplementary Materials: The following supporting information can be downloaded at: https://www.mdpi.com/article/10.3390/app15147981/s1, Figure S1: IR spectrum of **(BmIm)$_3$PMo$_{12}$O$_{40}$**, Figure S2: IR spectrum of **(BmIm)$_4$PMo$_{11}$VO$_{40}$**, Figure S3: IR spectrum of **(BuPyr)$_3$PMo$_{12}$O$_{40}$**, Figure S4: IR spectrum of **(BuPyr)$_4$PMo$_{11}$VO$_{40}$**, Figure S5: IR spectrum of **MRImd@PMo$_{12}$O$_{40}$**, Figure S6: IR spectrum of **MRImd@PMo$_{11}$VO$_{40}$**, Figure S7: IR spectrum of **MRPyr@PMo$_{12}$O$_{40}$**, Figure S8: IR spectrum of **MRPyr@PMo$_{11}$VO$_{40}$**, Figure S9: ^{1}H NMR spectrum of **(BmIm)$_3$PMo$_{12}$O$_{40}$** in dmso-d$_6$, Figure S10: ^{1}H NMR spectrum of **(BmIm)$_4$PMo$_{11}$V$_1$O$_4$** in dmso-d$_6$, Figure S11: ^{1}H NMR spectrum of **(BuPyr)$_3$PMo$_{12}$O$_{40}$** in dmso-d$_6$, Figure S12: ^{1}H NMR spectrum of **(BuPyr)$_4$PMo$_{11}$VO$_{40}$** in dmso-d$_6$, Figure S13: ^{13}C{^{1}H} NMR spectrum of **(BmIm)$_3$PMo$_{12}$O$_{40}$** in dmso-d$_6$, Figure S14: ^{13}C{^{1}H} NMR spectrum of **(BmIm)$_4$PMo$_{11}$V$_1$O$_4$** in dmso-d$_6$, Figure S15: ^{13}C{^{1}H} NMR spectrum

of **(BuPyr)$_3$PMo$_{12}$O$_{40}$** in dmso-d$_6$, Figure S16: ^{13}C{^{1}H} NMR spectrum of **(BuPyr)$_4$PMo$_{11}$VO$_{40}$** in dmso-d$_6$, Figure S17: ^{31}P{^{1}H} NMR spectrum of **(BmIm)$_3$PMo$_{12}$O$_{40}$** in dmso-d$_6$, Figure S18: ^{31}P{^{1}H} NMR spectrum of **(BmIm)$_4$PMo$_{11}$V$_1$O$_{40}$** in dmso-d$_6$, Figure S19: ^{31}P{^{1}H} NMR spectrum of **(BuPyr)$_3$PMo$_{12}$O$_{40}$** in dmso-d$_6$, Figure S20: ^{31}P{^{1}H} NMR spectrum of **(BuPyr)$_4$PMo$_{11}$V$_1$O$_{40}$** in dmso-d$_6$, Figure S21: ^{31}P and ^{13}C MAS NMR spectra of **MRImd@PMo$_{11}$VO$_{40}$** before and after the three catalytic runs.

Author Contributions: Conceptualization, methodology and validation, D.A., A.A.H.H. and P.G.; formal analysis and investigation, A.A.H.H.; resources, D.A. and P.G.; data curation, D.A. and A.A.H.H.; writing—original draft preparation, A.A.H.H.; writing—review and editing, D.A., A.A.H.H. and P.G.; supervision, project administration and funding acquisition, D.A. and P.G. All authors have read and agreed to the published version of the manuscript.

Funding: This work was funded by the CNRS, the Région Occitanie [Project GreenCatNat grant number N° 00138053/22009739], the IUT Toulouse Auch Castres and the IUT Chemistry Department and the Syndicat Mixte de la Communauté d'Agglomération Castres-Mazamet.

Data Availability Statement: The original contributions presented in this study are included in the article/Supplementary Materials. Further inquiries can be directed to the corresponding author.

Acknowledgments: The authors wish to acknowledge the CNRS and the IUT for their facilities. Yannick Coppel and Sandrine Vincendeau are warmly acknowledged for technical aspects.

Conflicts of Interest: The authors declare no conflict of interest.

Abbreviations

The following abbreviations are used in this manuscript:

aq	Aqueous
dec	Decane
TBHP	tert-butyl hydroperoxide
POM	Polyoxometalate
HPA	Heteropolyacid
BmIm	Butylmethyl imidazolium
BuPyr	Butyl pyridinium
Imd	Methyl imidazolium
Pyr	Pyridinium
MR	Merrifield resin

References

1. Faaij, A. Modern Biomass Conversion Technologies. *Mitig. Adapt. Strateg. Glob. Change* **2006**, *11*, 343–375. [CrossRef]
2. Ahorsu, R.; Medina, F.; Constantí, M. Significance and Challenges of Biomass as a Suitable Feedstock for Bioenergy and Biochemical Production: A Review. *Energies* **2018**, *11*, 3366. [CrossRef]
3. Dodds, D.R.; Gross, R.A. Chemicals from Biomass. *Science* **2007**, *318*, 1250–1251. [CrossRef] [PubMed]
4. Haveren, J.V.; Scott, E.L.; Sanders, J. Bulk Chemicals from Biomass. *Biofuels Bioprod. Biorefin.* **2008**, *2*, 41–57. [CrossRef]
5. Anastas, P.T.; Warner, J.C. *Green Chemistry: Theory and Practice*; Oxford University Press: Oxford, UK, 2000; ISBN 978-0-19-850698-0.
6. De, S.; Burange, A.S.; Luque, R. Conversion of Biomass-Derived Feedstocks into Value-Added Chemicals over Single-Atom Catalysts. *Green Chem.* **2022**, *24*, 2267–2286. [CrossRef]
7. Corma, A.; Iborra, S.; Velty, A. Chemical Routes for the Transformation of Biomass into Chemicals. *Chem. Rev.* **2007**, *107*, 2411–2502. [CrossRef] [PubMed]
8. Harman-Ware, A.E. Conversion of Terpenes to Chemicals and Related Products. In *Chemical Catalysts for Biomass Upgrading*; Crocker, M., Santillan-Jimenez, E., Eds.; Wiley: Hoboken, NJ, USA, 2020; pp. 529–568. ISBN 978-3-527-34466-6.
9. Geron, C.; Rasmussen, R.; Arnts, R.R.; Guenther, A. A Review and Synthesis of Monoterpene Speciation from Forests in the United States. *Atmos. Environ.* **2000**, *34*, 1761–1781. [CrossRef]
10. Behr, A.; Johnen, L. Myrcene as a Natural Base Chemical in Sustainable Chemistry: A Critical Review. *ChemSusChem* **2009**, *2*, 1072–1095. [CrossRef] [PubMed]

11. Taylor, A.J.; Linforth, R.S.T. (Eds.) *Food Flavour Technology*, 1st ed.; Wiley: Hoboken, NJ, USA, 2010; ISBN 978-1-4051-8543-1.
12. Behr, A.; Johnen, L.; Neubert, P. A Sustainable Route from the Renewable Myrcene to Methyl Ethersvia Direct Hydroalkoxylation. *Catal. Sci. Technol.* **2012**, *2*, 88–92. [CrossRef]
13. Fahlbusch, K.; Hammerschmidt, F.; Panten, J.; Pickenhagen, W.; Schatkowski, D.; Bauer, K.; Garbe, D.; Surburg, H. Flavors and Fragrances. In *Ullmann's Encyclopedia of Industrial Chemistry*; Wiley-VCH, Ed.; Wiley: Hoboken, NJ, USA, 2003; ISBN 978-3-527-30385-4.
14. Anastasiou, D.E. Investigating the Epoxidation of Poly-β-Myrcene: Optimization, Kinetics, and Thermodynamics. *J. Polym. Environ.* **2023**, *31*, 4044–4051. [CrossRef]
15. Asempour, F.; Yang, R.; Maric, M. Thermadapt Shape Memory Vitrimeric Polymyrcene Elastomer. *React. Funct. Polym.* **2024**, *201*, 105941. [CrossRef]
16. Ricci, G.; Boccia, A.C.; Palucci, B.; Sommazzi, A.; Masi, F.; Scoti, M.; De Stefano, F.; De Rosa, C. Synthesis of Stereoregular Polymyrcenes Using Neodymium-, Iron- and Copper-Based Catalysts. *Polym. Chem.* **2024**, *15*, 1367–1376. [CrossRef]
17. Li, T.; Zhang, M.; He, J.; Ni, P. Synthesis and Characterization of Graft Copolymers with Poly(ε-Caprolactone) Side Chain Using Hydroxylated Poly(β-Myrcene-Co-α-Methyl Styrene). *Molecules* **2024**, *29*, 2363. [CrossRef] [PubMed]
18. Ling, F.-W.; Luo, M.-C.; Chen, M.-K.; Zeng, J.; Li, S.-Q.; Yin, H.-B.; Wu, J.-R.; Xu, Y.-X.; Huang, G. Terminally and Randomly Functionalized Polyisoprene Lead to Distinct Aggregation Behaviors of Polar Groups. *Polymer* **2019**, *178*, 121629. [CrossRef]
19. Hahn, C.; Wagner, M.; Müller, A.H.E.; Frey, H. MyrDOL, a Protected Dihydroxyfunctional Diene Monomer Derived from β-Myrcene: Functional Polydienes from Renewable Resources via Anionic Polymerization. *Macromolecules* **2022**, *55*, 4046–4055. [CrossRef]
20. Sell, C.S. Terpenoids. In *Kirk-Othmer Encyclopedia of Chemical Technology*; Kirk-Othmer, Ed.; Wiley: Hoboken, NJ, USA, 2006; ISBN 978-0-471-48494-3.
21. Ma, S.-J.; Yu, J.; Yan, D.-W.; Wang, D.-C.; Gao, J.-M.; Zhang, Q. Meroterpene-like Compounds Derived from β-Caryophyllene as Potent α-Glucosidase Inhibitors. *Org. Biomol. Chem.* **2018**, *16*, 9454–9460. [CrossRef] [PubMed]
22. Machado, K.D.C.; Islam, M.T.; Ali, E.S.; Rouf, R.; Uddin, S.J.; Dev, S.; Shilpi, J.A.; Shill, M.C.; Reza, H.M.; Das, A.K.; et al. A Systematic Review on the Neuroprotective Perspectives of Beta-caryophyllene. *Phytother. Res.* **2018**, *32*, 2376–2388. [CrossRef] [PubMed]
23. Ahmed, A.F.; Su, J.-H.; Shiue, R.-T.; Pan, X.-J.; Dai, C.-F.; Kuo, Y.-H.; Sheu, J.-H. New β-Caryophyllene-Derived Terpenoids from the Soft Coral Sinularia n Anolobata. *J. Nat. Prod.* **2004**, *67*, 592–597. [CrossRef] [PubMed]
24. Giersch, W.K.; Boschung, A.F.; Snowden, R.L.; Schulte-Elte, K.H. Thermoconversion of Caryophyllene- to Farnesene-Type Sesquiterpenes. Short Access to the Enantiomers of (6*RS*,7*RS*)- and (6*RS*,7*SR*)-6,7-epoxy-6,7-dihydro-β-farnesenes. *Helv. Chim. Acta* **1994**, *77*, 36–40. [CrossRef]
25. Cheng, X.; Harzdorf, N.; Khaing, Z.; Kang, D.; Camelio, A.M.; Shaw, T.; Schmidt, C.E.; Siegel, D. Neuronal Growth Promoting Sesquiterpene-Neolignans; Syntheses and Biological Studies. *Org. Biomol. Chem.* **2012**, *10*, 383–393. [CrossRef] [PubMed]
26. Santos, P.S.; Oliveira, T.C.; Júnior, L.M.R.; Figueiras, A.; Nunes, L.C.C. β-Caryophyllene Delivery Systems: Enhancing the Oral Pharmacokinetic and Stability. *Curr. Pharm. Des.* **2018**, *24*, 3440–3453. [CrossRef] [PubMed]
27. Sköld, M.; Karlberg, A.-T.; Matura, M.; Börje, A. The Fragrance Chemical β-Caryophyllene—Air Oxidation and Skin Sensitization. *Food Chem. Toxicol.* **2006**, *44*, 538–545. [CrossRef] [PubMed]
28. Alberti, T.; Barbosa, W.; Vieira, J.; Raposo, N.; Dutra, R. (−)-β-Caryophyllene, a CB2 Receptor-Selective Phytocannabinoid, Suppresses Motor Paralysis and Neuroinflammation in a Murine Model of Multiple Sclerosis. *Int. J. Mol. Sci.* **2017**, *18*, 691. [CrossRef] [PubMed]
29. Mitzner, B.M.; Theimer, E.T.; Steinbach, L.; Wolt, J. α-Myrcene (2-Methyl-6-Methylene-1,7-Octadiene). *J. Org. Chem.* **1965**, *30*, 646–648. [CrossRef]
30. Gagan, S.; Sarang, K.; Rudzinski, K.J.; Liu, R.; Szmigielski, R.; Zhang, Y. Synthetic Strategies for Oxidation Products from Biogenic Volatile Organic Compounds in the Atmosphere: A Review. *Atmos. Environ.* **2023**, *312*, 120017. [CrossRef]
31. Barrero, A.F.; Molina, J.; Enrique Oltra, J.; Altarejos, J.; Barragán, A.; Lara, A.; Segura, M. Stereochemistry of 14-Hydroxy-β-Caryophyllene and Related Compounds. *Tetrahedron* **1995**, *51*, 3813–3822. [CrossRef]
32. Mahamat Ahmat, Y.; Kamkui, H.M.; Kaliaguine, S. Scaled up Epoxidation of Terpenes in Microemulsion. *Catal. Today* **2025**, *449*, 115202. [CrossRef]
33. Imperio, D.; Casali, E.; Del Grosso, E.; Caprioglio, D.; Minassi, A.; Panza, L. Trifluoromethyl Ketone Galactose Catalyst for Asymmetric Epoxidation: Experimental and Theoretical Model. *Eur. J. Org. Chem.* **2024**, *27*, e202301163. [CrossRef]
34. Cheng, X.; Harzdorf, N.L.; Shaw, T.; Siegel, D. Biomimetic Syntheses of the Neurotrophic Natural Products Caryolanemagnolol and Clovanemagnolol. *Org. Lett.* **2010**, *12*, 1304–1307. [CrossRef] [PubMed]
35. Shi, L.; Mao, W.; Zhang, L.; Zhao, Y.; Huang, H.; Xiao, Y.; Mao, L.; Fu, Z.; Yu, N.; Yin, D. An Ultrathin Amino-Acid Based Copper(II) Coordination Polymer Nanosheet for Efficient Epoxidation of β-Caryophyllene. *Mol. Catal.* **2021**, *511*, 111754. [CrossRef]

36. Li, S.; Shi, L.; Zhang, L.; Huang, H.; Xiao, Y.; Mao, L.; Tan, R.; Fu, Z.; Yu, N.; Yin, D. Ionic Liquid-Mediated Catalytic Oxidation of β-Caryophyllene by Ultrathin 2D Metal-Organic Framework Nanosheets under 1 Atm O_2. *Mol. Catal.* **2020**, *496*, 111196. [CrossRef]
37. Dileep, R.; Rudresha, B.J. An Ionic Liquid Immobilized Copper Complex for Catalytic Epoxidation. *RSC Adv.* **2015**, *5*, 65870–65873. [CrossRef]
38. Yamazaki, S. An Effective Procedure for the Synthesis of Acid-Sensitive Epoxides: Use of 1-Methylimidazole as the Additive on Methyltrioxorhenium-Catalyzed Epoxidation of Alkenes with Hydrogen Peroxide. *Org. Biomol. Chem.* **2010**, *8*, 2377. [CrossRef] [PubMed]
39. Salles, L.; Brégeault, J.-M.; Thouvenot, R. Comparison of Oxoperoxophosphatotungstate Phase Transfer Catalysis with Methyltrioxorhenium Two-Phase Catalysis for Epoxidation by Hydrogen Peroxide. *C. R. Acad. Sci. Ser. IIC Chem.* **2000**, *3*, 183–187. [CrossRef]
40. Mahha, Y.; Salles, L.; Piquemal, J.-Y.; Briot, E.; Atlamsani, A.; Brégeault, J.-M. Environmentally Friendly Epoxidation of Olefins under Phase-Transfer Catalysis Conditions with Hydrogen Peroxide. *J. Catal.* **2007**, *249*, 338–348. [CrossRef]
41. Tibbetts, J.D.; Cunningham, W.B.; Vezzoli, M.; Plucinski, P.; Bull, S.D. Sustainable Catalytic Epoxidation of Biorenewable Terpene Feedstocks Using H_2O_2 as an Oxidant in Flow Microreactors. *Green Chem.* **2021**, *23*, 5449–5455. [CrossRef]
42. Cunningham, W.B.; Tibbetts, J.D.; Hutchby, M.; Maltby, K.A.; Davidson, M.G.; Hintermair, U.; Plucinski, P.; Bull, S.D. Sustainable Catalytic Protocols for the Solvent Free Epoxidation and Anti-Dihydroxylation of the Alkene Bonds of Biorenewable Terpene Feedstocks Using H_2O_2 as Oxidant. *Green Chem.* **2020**, *22*, 513–524. [CrossRef]
43. Escande, V.; Petit, E.; Garoux, L.; Boulanger, C.; Grison, C. Switchable Alkene Epoxidation/Oxidative Cleavage with H_2O_2/$NaHCO_3$: Efficient Heterogeneous Catalysis Derived from Biosourced Eco-Mn. *ACS Sustain. Chem. Eng.* **2015**, *3*, 2704–2715. [CrossRef]
44. Evtushok, V.Y.; Ivanchikova, I.D.; Lopatkin, V.A.; Maksimchuk, N.V.; Podyacheva, O.Y.; Suboch, A.N.; Stonkus, O.A.; Kholdeeva, O.A. Heterolytic Alkene Oxidation with H_2O_2 Catalyzed by Nb-Substituted Lindqvist Tungstates Immobilized on Carbon Nanotubes. *Catal. Sci. Technol.* **2021**, *11*, 3198–3207. [CrossRef]
45. Shen, Y.; Jiang, P.; Wai, P.; Gu, Q.; Zhang, W. Recent Progress in Application of Molybdenum-Based Catalysts for Epoxidation of Alkenes. *Catalysts* **2019**, *9*, 31. [CrossRef]
46. Cherevan, A.S.; Nandan, S.P.; Roger, I.; Liu, R.; Streb, C.; Eder, D. Polyoxometalates on Functional Substrates: Concepts, Synergies, and Future Perspectives. *Adv. Sci.* **2020**, *7*, 1903511. [CrossRef] [PubMed]
47. Tarlani, A.; Abedini, M.; Nemati, A.; Khabaz, M.; Amini, M.M. Immobilization of Keggin and Preyssler Tungsten Heteropolyacids on Various Functionalized Silica. *J. Colloid Interface Sci.* **2006**, *303*, 32–38. [CrossRef] [PubMed]
48. Wang, Y.; Gayet, F.; Guillo, P.; Agustin, D. Organic Solvent-Free Olefins and Alcohols (Ep) Oxidation Using Recoverable Catalysts Based on $[PM_{12}O_{40}]^{3-}$ (M = Mo or W) Ionically Grafted on Amino Functionalized Silica Nanobeads. *Materials* **2019**, *12*, 3278. [CrossRef] [PubMed]
49. Gupta, K.C.; Kumar Sutar, A.; Lin, C.-C. Polymer-Supported Schiff Base Complexes in Oxidation Reactions. *Coord. Chem. Rev.* **2009**, *253*, 1926–1946. [CrossRef]
50. Pisk, J.; Agustin, D. Molybdenum, Vanadium, and Tungsten-Based Catalysts for Sustainable (Ep) Oxidation. *Molecules* **2022**, *27*, 6011. [CrossRef] [PubMed]
51. Tsigdinos, G.A.; Hallada, C.J. Molybdovanadophosphoric Acids and Their Salts. I. Investigation of Methods of Preparation and Characterization. *Inorg. Chem.* **1968**, *7*, 437–441. [CrossRef]
52. Pisk, J.; Agustin, D.; Poli, R. Organic Salts and Merrifield Resin Supported $[PM_{12}O_{40}]^{3-}$ (M = Mo or W) as Catalysts for Adipic Acid Synthesis. *Molecules* **2019**, *24*, 783. [CrossRef] [PubMed]
53. Hioki, H.; Ooi, H.; Hamano, M.; Mimura, Y.; Yoshio, S.; Kodama, M.; Ohta, S.; Yanai, M.; Ikegami, S. Enantioselective Total Synthesis and Absolute Stereostructure of Hippospongic Acid A. *Tetrahedron* **2001**, *57*, 1235–1246. [CrossRef]
54. Noorhisham, N.A.; Amri, D.; Mohamed, A.H.; Yahaya, N.; Ahmad, N.M.; Mohamad, S.; Kamaruzaman, S.; Osman, H. Characterisation Techniques for Analysis of Imidazolium-Based Ionic Liquids and Application in Polymer Preparation: A Review. *J. Mol. Liq.* **2021**, *326*, 115340. [CrossRef]
55. Lawrenson, S.; North, M.; Peigneguy, F.; Routledge, A. Greener Solvents for Solid-Phase Synthesis. *Green Chem.* **2017**, *19*, 952–962. [CrossRef]
56. Mitsuaki, K.; Hiroyuki, M.; Yukiko, M.; Yoshiyasu, F. Convenient Synthesis of Chiral Epoxyisoprenoids by Yeast Reduction. *Tetrahedron Lett.* **1990**, *31*, 4025–4026. [CrossRef]
57. Runckel, W.J.; Goldblatt, L.A. Inhibition of Myrcene Polymerization during Storage. *Ind. Eng. Chem.* **1946**, *38*, 749–751. [CrossRef]
58. Keller, C.L.; Walkling, C.J.; Zhang, D.D.; Baldwin, L.C.; Austin, J.S.; Harvey, B.G. Designer Biosynthetic Jet Fuels Derived from Isoprene and α-Olefins. *ACS Sustain. Chem. Eng.* **2023**, *11*, 4030–4039. [CrossRef]
59. Kafuku, K.; Oyamada, T.; Nishi, M. A NEW DITERPENE—γ-CAMPHORENE. *Bull. Chem. Soc. Jpn.* **1933**, *8*, 144–148. [CrossRef]

60. Francomano, F.; Caruso, A.; Barbarossa, A.; Fazio, A.; La Torre, C.; Ceramella, J.; Mallamaci, R.; Saturnino, C.; Iacopetta, D.; Sinicropi, M.S. β-Caryophyllene: A Sesquiterpene with Countless Biological Properties. *Appl. Sci.* **2019**, *9*, 5420. [CrossRef]
61. Gyrdymova, Y.V.; Rubtsova, S.A. Caryophyllene and Caryophyllene Oxide: A Variety of Chemical Transformations and Biological Activities. *Chem. Pap.* **2022**, *76*, 1–39. [CrossRef]
62. Cederbaum, A.I.; Qureshi, A.; Cohen, G. Production of Formaldehyde and Acetone by Hydroxyl-Radical Generating Systems during the Metabolism of Tertiary Butyl Alcohol. *Biochem. Pharmacol.* **1983**, *32*, 3517–3524. [CrossRef] [PubMed]
63. Lin, C.C.; Smith, F.R.; Ichikawa, N.; Baba, T.; Itow, M. Decomposition of Hydrogen Peroxide in Aqueous Solutions at Elevated Temperatures. *Int. J. Chem. Kinet.* **1991**, *23*, 971–987. [CrossRef]
64. Haidar, A.A.H.; Agustin, D. Role of Organic Solvent and Influence of Oxidant in the Oxidation of Linalool Catalyzed by Molybdenum and Vanadium Complexes. *Tetrahedron Green Chem.* **2023**, *2*, 100029. [CrossRef]